Space weathering from Mercury to the asteroid belt

Bruce Hapke

Department of Geology and Planetary Science, University of Pittsburgh, Pittsburgh, Pennsylvania

Abstract. The variety of evidence bearing on the nature of space weathering is reviewed. The effects of space weathering include spectral darkening, reddening and subdued absorption bands, and the distinctive magnetic electron spin resonance caused by single-domain metallic iron particles. Ever since the Apollo missions, two paradigms have dominated the thinking of the planetary science community concerning space weathering: (1) the optical effects are caused by impact-vitrified glass in agglutinates, and (2) the submicroscopic metallic iron results from the reduction of ferrous iron by the impact melting of minerals whose surfaces have been saturated with hydrogen from the solar wind. However, studies carried out since the Apollo program showed that both of these paradigms are invalid. A hypothesis first suggested by the author and his colleagues 26 years ago, but not generally accepted at that time, now appears to be essentially correct: Both the optical and magnetic effects are caused by metallic iron particles smaller than the wavelength in ubiquitous vapor-deposited coatings on soil particle surfaces and inside agglutinates. The vapor is generated by both solar wind sputtering and micrometeorite impact vaporization and injected preferentially downward into the porous regolith. The iron is reduced by a physical process, the selective loss of oxygen that occurs during deposition of the vapor, and does not require heating, melting, or a reducing environment. A mathematical theory that describes the optical effects of the submicroscopic iron quantitatively is derived and applied to the regoliths of the Moon, Mercury and an S asteroid.

1. Introduction

Space weathering is the aggregate of the physical and chemical changes that occur to material exposed on the surface of an airless body. The space environment is often thought to be inert. However, micrometeorites and particulate and electromagnetic radiation bombard the surfaces of bodies without atmospheres and can have important effects on their regoliths. Space weathering is of considerable interest to scientists who study planets by remote sensing because it causes major changes in the optical properties of the surfaces. On the Moon, space weathering lowers the albedo, reddens the spectral slope, obscures absorption bands, and generates the characteristic magnetic electron spin resonance of the lunar regolith. These changes are the subject of this paper. It will be shown that they result from the production of submicroscopic metallic iron (SMFe) in the regolith by deposition of vapors created by micrometeorite impact vaporization and solar wind sputtering. (Some authors use the phrase "nanophase metallic iron", abbreviated npFe⁰, to refer to the carrier of the space weathering. However, this phrase connotes iron particles a few nanometers in diameter, whereas a large fraction of the iron particles that cause the space weathering effects in the lunar soil are tens and hundreds of nanometers in size. It will be shown that these particles are just as important to the optical effects as the nanometer-sized particles that are the primary

carriers of the ferromagnetic resonance of the soil. Hence, "submicroscopic metallic iron", abbreviated SMFe, is preferred.) This vapor phase transport also causes measureable chemical effects.

One of the first persons to point out that a darkening process operates on the Moon was T. Gold. In a classic paper, *Gold* [1955] argued that only craters that are judged to be young on the basis of stratigraphic relationships have rays and, therefore, that rays are ephemeral features whose optical properties gradually change to those of their surroundings. This was also emphasized by *Hapke and Van Horn* [1963]. Gold's prediction was amply confirmed when Apollo 11 samples were brought from the Moon, and it was found that the lunar soil was much darker than pulverized rocks of the same composition [*Conel and Nash*, 1970; *Gold et al.*, 1970; *Hapke et al.*, 1970].

(Gold's paper should be read by all serious students of the history of planetary science. Although he was an astronomer and had no formal training in geology, he instinctively used the principal tools of the geologist, uniformitarianism and stratigraphy, to arrive at major conclusions about the nature of the lunar surface well before the Apollo missions. He argued that the lunar craters are impact features and that presently the Moon is geologically dead. Invoking uniformitarianism, he argued that the Moon always has been dead and, therefore, the maria could not be lava flows. Instead he suggested that they were deep deposits of fine-grained powder ["dust" to an astronomer] that had been eroded from elevated areas and carried downhill into depressions by an electrostatic levitation process. He pointed out that only those craters that

are judged to be young on the basis of degree of degradation, density of smaller craters on their interiors, and overlapping relationships have rays. Therefore a darkening process must be operating on the lunar surface, which he suggested was the reason the maria have low albedos. Gold's paper has been ridiculed in some quarters on the grounds that it predicted that spacecraft and astronauts would sink out of sight into the dust. However, such a statement does not appear in his paper, although by analogy with snow-covered glacial crevasses, he did suggest this as a possibility in later lectures and articles in the popular press. Although his prediction about the nature of the maria turned out to be incorrect, in retrospect, his paper was remarkably prescient: Lunar craters are the result of impacts; the Moon's surface is covered with a fine-grained regolith; erosion does occur on the lunar surface; a darkening process is operating; and electrostatic levitation occurs [Zook and McCoy, 1991], although not at the rate he envisioned.)

During the Apollo era a large body of experimental work on both lunar samples and laboratory analogs relevent to space weathering was carried out. In sections 2 - 5 of this paper these and more recent results are reviewed and their significance critically evaluated. In section 6 the various hypotheses for the origin of the critical SMFe are assessed. It will be shown that vapor deposition is the only known geological process that has been demonstrated to produce the SMFe. The vapor - deposition model is further elaborated in section 7. In section 8 a mathematical theory of the optical effects of space weathering is derived and applied to the surfaces of the Moon and Mercury and to the problem of the connection between ordinary chondrites and S - asteroids.

2. Characteristic Size Parameters of the Lunar Regolith

2.1. Introduction

The lunar regolith has a wide distribution of particle sizes. As a result, the mass-weighted and area-weighted median sizes are markedly different. Although the former is of interest to petrologists and geochemists, the latter is important to the spectral reflectance because the smaller sizes dominate the optical properties of a medium with a wide size distribution, a fact that has often not been fully appreciated. The radiative transfer equation, which governs the optical properties of a particulate medium, contains factors such as the scattering and absorption coefficients that are proportional to the cross-sectional areas of the particles. Hence the optical properties are strongly dependent on the size weighted by particle cross-sectional area, not mass. Evidence will be given in succeeding sections that space weathering is caused by ubiquitous, light-absorbing coatings on the grain surfaces. Such coatings affect the smaller particles much more than the larger ones because of the greater surface/volume ratio. In this section the various quantities that charactize the size distribution of the lunar regolith are given. Also, some of these parameters will be needed later in the quantitative models of section 8.

2.2. Mass-Weighted Median Size

Let the median grain size weighted by mass be D_M. This is the size such that equal amounts of mass are in grains larger

and smaller than D_M, and is around 70 μm for most mature soils [Carrier et al., 1991; Heiken et al., 1991].

2.3. Particle Size Distribution

If a soil sample is sifted into different size fractions and the mass of particles larger than a given sieve size plotted against the logarithm of size, it is found that the points fall approximately on a straight line with a slope of -1 (Figure 1); that is, the mass in particles greater than a certain size decreases proportionally to the logarithm of the size. This requires that the number of particles between D and $D+dD$ be of the form

$$N(D) = CD^{-4},$$

where C is a constant. Then the mass of soil in particles larger than D is

$$M(>D) = \int_D^{D_U} \rho\pi\frac{D^3}{6}N(D)dD = \frac{C\pi\rho}{6}\ln(\frac{D_U}{D}) \qquad (1)$$

where D_U is the upper limit to the size distribution and ρ is the density of a particle. This has $M(>D)$ proportional to $-\ln(D)$, as observed.

However, this distribution is somewhat misleading for two reasons. First, it tends to underestimate the number of small particles because they cling to larger particles during sieving. Second, a large fraction of the soil grains are agglutinates: composite mixtures of smaller particles of minerals and glass weakly sintered together. Many of the agglutinates are so poorly consolidated that they fall apart if handled, so that there is considerable ambiguity as to what constitutes a soil particle. Gold et al. [1970] used water - column sedimentation and scanning electron microscope (SEM) techniques and found that there are more smaller particles than would be estimated from dry sieving.

The upper limit of the Apollo soil samples is known because they were passed through a 1 mm sieve prior to distribution to investigators. Hence D_U = 1000 μm. Although the lower limit is ill - defined for the reasons discussed above, an effective lower size limit D_L can be found by requiring that the total mass between D_L and D_M equal the total mass between D_M and D_U. This requires

$$\int_{D_L}^{D_M} \rho\pi\frac{D^3}{6}N(D)dD = \int_{D_M}^{D_U} \rho\pi\frac{D^3}{6}N(D)dD, \qquad (2)$$

which gives

$$\ln(D_M/D_L) = \ln(D_U/D_M).$$

Solving this for D_L and taking D_M = 70 μm gives
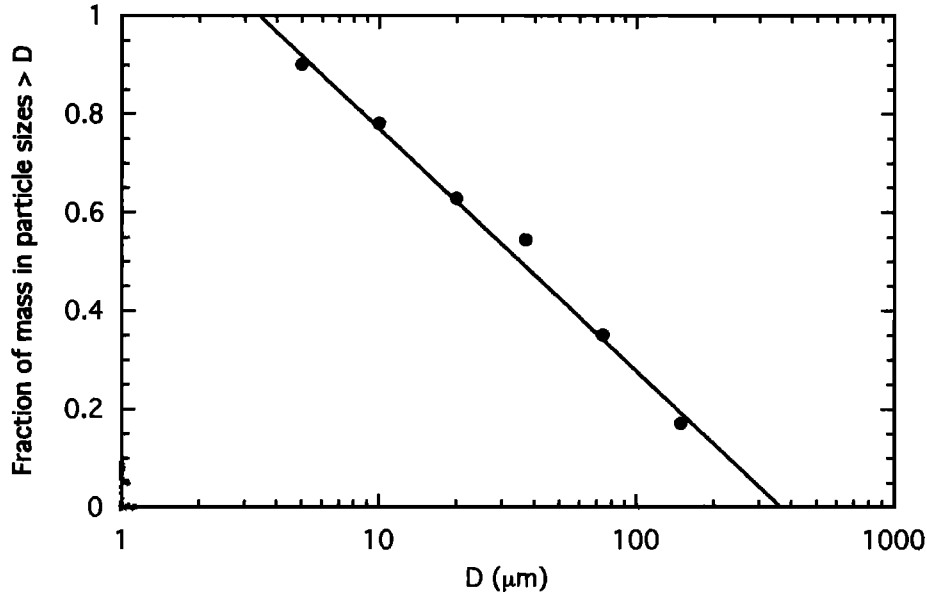
$$D_L = D_M^2/D_U = 4.9 \approx 5 \text{ μm.}$$

Figure 1. Cumulative particle size distribution of lunar soil sample 10084 [*Hapke et al.*, 1970], measured by wet - sieving in distilled water. The solid circles are the data; the line has a slope of -1.

2.4. Area-Weighted Median Size

The median size D_A such that half the area is in particle sizes $> D_A$ and half in particle sizes $< D_A$ may be defined similarly to D_M:

$$\int_{D_L}^{D_A} N(D)\sigma(D)dD = \int_{D_A}^{D_U} N(D)\sigma(D)dD \qquad (3)$$

where $\sigma(D) = \pi D^2/4$ is the cross-sectional area of a particle of size D. Evaluating these integrals gives

$$1/D_L\text{-}1/D_A = 1/D_A\text{-}1/D_U ,$$

which may be solved for D_A :

$$D_A = 2D_U D_L/(D_U\text{-}D_L) \approx 2D_L = 10 \ \mu m,$$

since $D_L \ll D_U$. The significance of the area-weighted median size can be appreciated from the fact that half of the light incident on the regolith encounters particles smaller than 10 μm in size.

2.5. Area-Weighted Mean Size

Another parameter that is important for the optical properties of the medium is the mean optical thickness of a particle $\tau_p = ED_p$, where E is the extinction coefficient inside a typical particle and D_p is the mean size weighted by cross-sectional area. This parameter is significant because it characterizes the single scattering albedo of a typical particle in the medium which, in turn, determines the reflectance. The mean size weighted by area is

$$D_p = \frac{\int_{D_L}^{D_U} N(D)\sigma(D)D\,dD}{\int_{D_L}^{D_U} N(D)\sigma(D)dD} = \frac{\int_{D_L}^{D_U} \frac{dD}{D}}{\int_{D_L}^{D_U} \frac{dD}{D^2}}$$

$$= \frac{\ln(\frac{D_U}{D_L})}{\frac{1}{D_L}-\frac{1}{D_U}} \approx D_L\ln(\frac{D_U}{D_L}) = 26 \ \mu m , \qquad (4)$$

since $D_L \ll D_U$.

2.6. Specific Surface Area Equivalent Size

The specific surface area (SSA), the surface area per unit mass, was measured for several soil samples using standard gas adsorption methods [*Cadenhead et al.*, 1977]. Typical values for a mature soil are around 5000 cm^2 gm^{-1}. If the soil consisted of spherical particles of a single size D and with density 3 gm cm^{-3}, then SSA = $\pi D^2/[\rho\pi D^3/6]$ = 2/D, so that the diameter of the equivalent spheres would be D = 2/SSA = 4 μm, which is smaller than most of the particles in the distribution. This high SSA is interpreted to result from the fact that the agglutinates tend to have highly irregular shapes with many reentrant cavities.

3. Optical Properties of the Lunar Regolith

A typical sample of lunar soil has a spectrum that increases monotonically with wavelength and displays weak absorption bands at wavelengths around 1 and 2 μm. Compared with pulverized rock of similar composition from the same Apollo site, the lunar regolith has a lower albedo, reddened spectrum, and subdued absorption bands [*Adams and Jones*, 1970; *Hapke et al.*, 1970]. This is illustrated in Figure 2. The goal of this paper is to explain these differences.
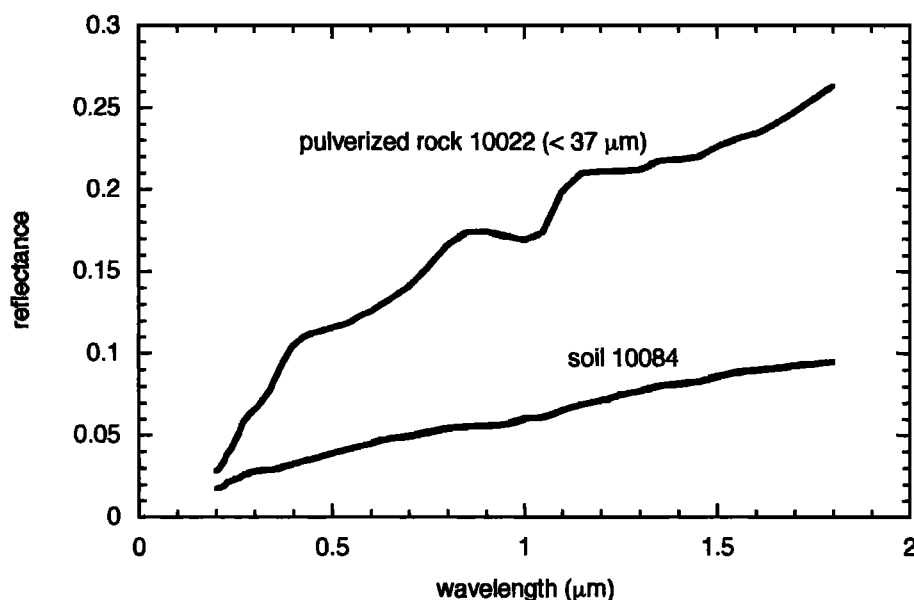
Figure 2. Bidirectional reflectance spectra ($i = e = 30°$, $g = 60°$, where i is the incidence angle, e is the viewing angle and g is the phase angle), relative to a MgO standard, of Apollo 11 lunar soil sample 10084 and lunar rock 10022 pulverized to < 37 μm.

In order to facilitate the understanding of the effects of space weathering, the optical properties of the major minerals in the lunar regolith will be reviewed in this section.

The most important minerals in Apollo lunar samples are olivine, high-Ca clinopyroxene (augite), high-Ca plagioclase feldspar (anorthite), and Fe-Ti oxide (ilmenite). In addition, lunar soil contains abundant glass, mostly in agglutinates, made by impact vitrification and by deposition of impact generated vapor. The fraction of agglutinatic glass increases as the particle size decreases [*Taylor et al.*, 1999b]. The fraction of feldspathic minerals also increases with decreasing size [*Papike et al.*, 1982], probably because they are more friable than the other common lunar minerals.

Fischer and Pieters [1994] measured the spectra of separated sizes and found that, as is typical for nonopaque powders, the reflectance decreases as the particle size increases. The spectra of the bulk soil are intermediate between the spectra of the < 25 μm and 25-45 μm separates (Figure 3). This can be understood from the fact that the median size weighted by cross-sectional area is about $D_p = 26$ μm (section 2.5). In addition, Fischer and Pieters found that the <10 μm size fraction has a different spectrum than the bulk: Instead of increasing approximately linearly with wavelength, the spectrum of the smallest size fraction is convex - upward and exhibits very small or no absorption bands.

The silicate minerals are dominated by two sets of extremely strong absorption band systems: an exiton/valence-conduction transition band system below 200 nm and vibrational reststrahlen bands near 10 μm. Only relatively weaker bands exist between these strong bands. Hence the reflectances of powdered siilcates are fairly high in near-ultraviolet, visible, and near-infrared wavelengths, where most

remote sensing observations are made. The wing of the far - UV band system causes the reflectances of silicate powders to decrease with decreasing wavelength in the near UV. The reststrahlen bands cause silicate minerals to have high emissivities in the thermal IR. The reflectance spectra of the major lunar minerals in powder form are shown in Figure 4.

The most useful absorption band for remote sensing has been the one near 1000 nm in the silicates and is caused by the excitation of an electron on Fe^{2+} surrounded by six oxygen ions [*Burns*, 1970; *Adams*, 1975]. This band is forbidden and, hence, is relatively weak. The band center is at 900 nm in low-Ca pyroxenes and moves toward longer wavelengths as the Fe-O distances are increased by the addition of Ca. In olivine this band occurs as a broad composite of three unresolved bands slightly longward of 1000 nm. In anorthite the band is at 1250 nm. Pyroxene has a second, weak ferrous band near 2000 nm, but olivine and plagioclase do not.

A much stronger silicate Fe band occurs at 260 nm [*Wells and Hapke*, 1977] and can be seen as an inflection on the shoulder of the far-UV band in the spectrum of anorthite in Figure 4. Because this band is below the ozone cutoff of the Earth's atmosphere, it has not been utilized for remote sensing of planetary surfaces. This band is an iron - oxygen charge-transfer band in which one of the outer electrons on the iron ion is excited into a higher molecular orbital level in the Fe^{2+}-O^{2-} system. The band is an allowed transition and, hence, is relatively strong. Consequently, most minerals have low reflectances in the near UV even if only trace amounts of Fe^{2+} are present.

Augite can incorporate a small amount of Ti^{4+} in its lattice. This ion interacts with Fe^{2+} present to cause a charge - transfer band at 340 nm in Ti-bearing clinopyroxenes, in which the absorption of a photon excites an electron on Fe^{2+} to a higher
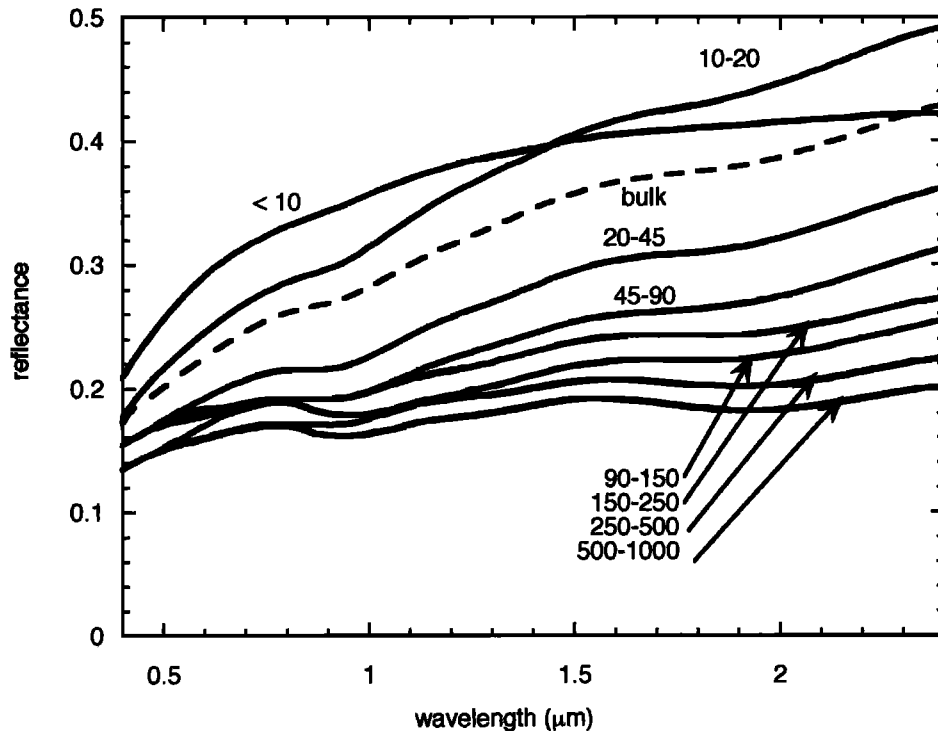
Figure 3. Bidirectional reflectance spectra ($i = 30°$, $e = 0$, $g = 30°$, relative to a polytetrafluoroethylene (PFE) standard) of seprated size fractions (in μm) of lunar soil sample 67701 [*Fischer and Pieters*, 1994]. The fractions were wet - sieved in liquid freon. Subsequent investigation [*Noble et al.*, 2001] showed that soaking a silicate powder in freon affected its spectrum in such a way as to change the amplitude, but not the general shape of the reflectance curve. (Data generously furnished by C. Pieters.)

level in the Fe^{2+}-Ti^{4+} system, leaving the iron in the Fe^{3+} state and the titanium as Ti^{3+} [*Cohen*, 1972].

Because the silicate minerals are transparent in the near - UV/visible/near - IR, the major contributors to their optical properties are photons that have penetrated into the interiors of the minerals and scattered back out, so that an absorption band is seen as a minimum in reflectance. By contrast, ilmenite is a nearly opaque mineral whose optical characteristics are controlled by Fresnel reflection from its surface. Hence the reflectance of ilmenite is low and the two charge - transfer
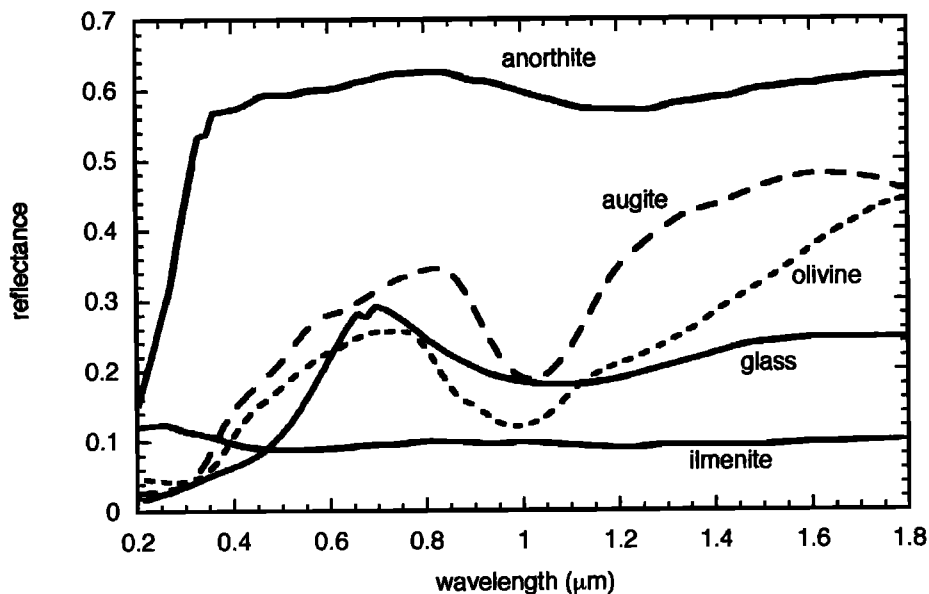

Figure 4. Bidirectional reflectance spectra ($i = e = 30°$, $g = 60°$, relative to a BaSO$_4$ standard) of the major minerals found on the lunar surface, pulverized to < 74 μm (data from *Wagner et al.* [1987]).

absorption bands at 260 and 340 nm are seen as maxima, rather than minima. The spectrum of a terrestrial ilmenite powder is shown in Figure 4. In addition to the two charge transfer bands, this specimen also has a band at 800 nm due to Fe^{3+} impurities which are not present in lunar ilmenite

Glass is abundant in the lunar regolith. Figure 4 also shows the spectrum of an artificial powdered glass of the same composition as Apollo 11 lunar basalt [*Wells and Hapke*, 1977]. The glass was made from reagent - grade oxides melted in a high vacuum and is free of Fe^{3+}. The glass has the same absorption bands displayed by the lunar rock at 260, 340, 1000, and 2000 nm. An additional band, which is not present in the rock, is a second Fe-Ti charge-transfer band at 430 nm. This latter band can make a high-Ti glass have a steep slope between 400 and 700 nm so that the glass appears red to the eye. (In fact, a high-Ti, glass-rich soil at the Taurus-Littrow region of the Moon was initially misidentified as hematite by the Apollo 17 astronauts.) However, the glass shown in Figure 4 is not dark, particularly between 600 and 800 nm, and its overall spectral slope is not red. It also has strong absorption bands because much of the Fe and Ti in a crystalline rock of equivalent composition are in the interiors of the ilmenite grains, where they are effectively invisible, whereas in a glass these ions are in the transparent silicate matrix, where they can take part in the absorption process to produce bands that are stronger than those of the rocks. The glass bands are much broader than the rock bands because the lattice sites are distorted in the glass and have a variety of cation-anion distances.

4. Laboratory Experiments That Attempted to Simulate Space Weathering

4.1. Introduction

During the past quarter century a large number of experiments that attempted to duplicate one aspect or another of

the space environment were carried out in order to simulate space weathering in the laboratory. These included melting to simulate meteorite impact vitrification, irradiation by kilovolt H and He ions to simulate effects of the solar wind, and vapor deposition to simulate impact vaporization effects. These experiments will be critically reviewed in this section. Since the Apollo missions, discussions of space weathering have been dominated by the assumption that it is due to vitrification. It will be shown that the experimental basis for this assumption is highly suspect and that the other two processes have much stronger experimental and theoretical support.

4.2. Vitrification Experiments

When the first samples of lunar soil were brought to Earth by the Apollo 11 mission, it was found that they contained abundant particles of dark glass, chiefly in the agglutinates. *Conel and Nash* [1970] made the reasonable suggestion that vitrification of lunar rocks by meteorite impacts was the cause of lunar darkening. They melted a lunar rock and produced a material that was dark and reddish with subdued absorption bands, which appeared to confirm their hypothesis. *Adams and McCord* [1971] repeated the experiment with the same result (Figure 5). Since that time it has been a virtual paradigm within the planetary science community that the optical effects of space weathering are due to impact vitrification.

However, Hapke and his colleagues attempted to repeat these experiments, but with dramatically different results [*Hapke et al.*, 1975a; *Cassidy and Hapke*, 1975]. When they vitrified lunar rocks in a vacuum the resulting glasses had high albedos, flat spectra, and strong absorption bands (figure 6). *Mao et al.* [1973] measured the spectra of synthetic lunar glasses prepared under carefully controlled reducing conditions in a hydrogen atmosphere and.of glasses from lunar soil The absorption spectra of their glasses were very similar to those of *Hapke et al.* [1975a].
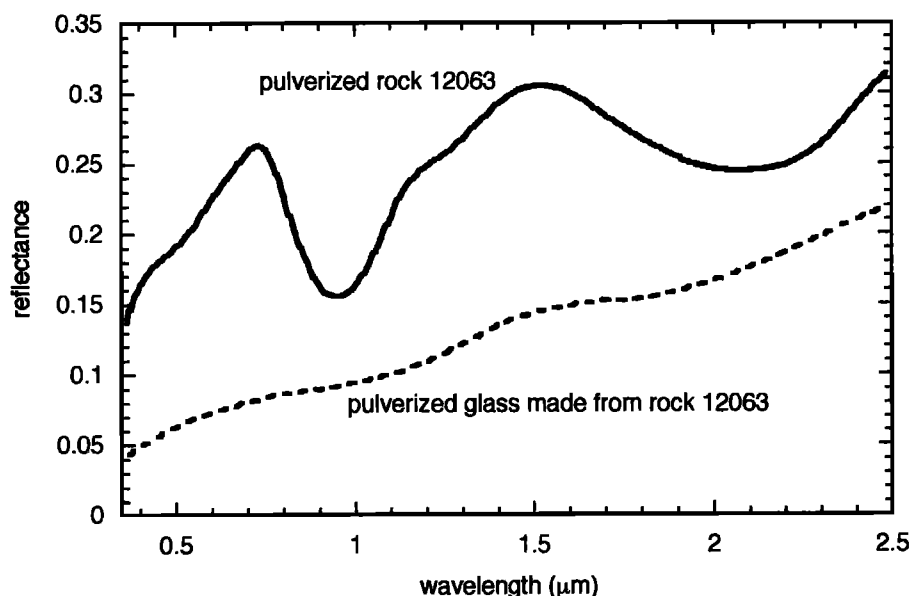

Figure 5. Hemispherical reflectance spectra (relative to an MgO standard) of lunar rock 12063 and glass made by melting the same rock in N_2, both pulverized to 125-500 μm (data from *Adams and McCord* [1971]).
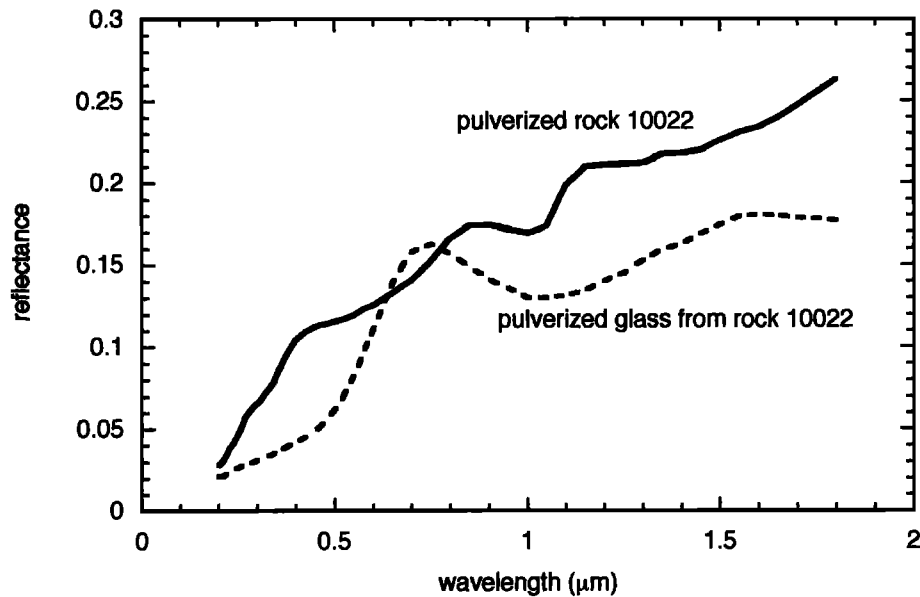
Figure 6. Bidirectional reflectance spectra ($i = e = 30°$, $g = 60°$, relative to a $BaSO_4$ standard) of lunar rock 10022 and glass made by melting the same rock in vacuo, both pulverized to < 37 μm.

After a detailed investigation *Wells and Hapke* [1977] showed that the reason for the discrepancies very probably was the differing environments in which the vitrifications were carried out, which caused the Fe in the samples to have different valence states. *Conel and Nash* [1970] and *Adams and McCord* [1971] had melted their samples in a Pt crucible in flowing commercial N_2 gas at 1 atm pressure, whereas *Hapke et al.* [1975a] had melted their lunar rocks in a high vacuum, reasoning that this was the best terrestrial analog to lunar vitrification conditions. Commercial N_2 typically contains of the order of 0.1% impurities, chiefly O_2 and H_2O. Such an environment is well above the $FeO-Fe_2O_3$ phase boundary and, hence, is highly oxidizing. In addition, a Pt crucible can act as a catalyst in the reaction $Fe^{2+} \longrightarrow Fe^0 + Fe^{3+}$, with the Fe^0 alloying with the Pt [*Cassidy and Hapke*, 1975]. Ferric iron has strong allowed absorption bands in the visible part of the spectrum.

Thirty years after the fact one can only speculate. However, it is highly likely that the apparent glasses made by Conel-Nash and Adams-McCord were dark and red because they contained microscopic precipitates of ferric-bearing minerals, such as magnetite, maghemite and hematite. None of these authors reported examining their materials in polarized light under petrographic microscopes, so it is unclear whether or not their samples were true glasses. *Wells and Hapke* [1977] characterized their glasses by petrographic examination, wet chemical methods, and Mossbauer spectroscopy. Their glasses that were ferric-free had high albedos and strong bands. The only way they were able to make glasses that were dark and reddish at all wavelengths and with subdued absorption bands was by melting under oxidizing conditions.

Clark et al. [1992] investigated the hypothesis that vitrification might account for the spectral differences between ordinary chondrites and S - asteroids by melting several meteorites. However, they also carried out their experiments in a N_2 atmosphere and Pt crucible, so that their atmospheric environment probably was oxidzing. If the environment had been reducing during melting, the metallic Ni-Fe in the meteorites would have separated from the silicate because the two liquids are immiscible. This should have resulted in considerable difficulty grinding up the sample after resolidification. However, Clark et al. did not report any such problems, which suggests that the meteoritic metal had been oxidized.   On the other hand, the glasses were not appreciably darker or redder than the starting meteorites. Thus it is likely that the metal in the meteorites acted as a buffer which prevented the glass from being overoxidized to the same extent as the glasses in the experiments of Conel-Nash and Adams-McCord.

Cloutis and Gaffey [1993] measured the spectra of several glasses made by melting terrestrial igneous rocks. Rock samples were placed in Pt crucibles and heated (apparently in air) to 1000° C to drive off water and then vitrified at 1400° C for 15 min in a CO_2-CO atmosphere. The glass was darker and redder than the parent rock.   In spite of the reducing melting environment, chemical analysis of the glasses showed that they all contained abundant amounts of ferric iron, as much as 14% in some cases. Thus these glasses are poor analogs to lunar glasses.

To summarize the results of the vitrification experiments: it is likely that the glasses of *Conel and Nash* [1970] and *Adams and McCord* [1971] were melted under oxidizing conditions so that they contained large amounts of Fe^{+3}, like the glasses of *Cloutis and Gaffey* [1993]. Ferric iron has strong absorption bands in the visible portion of the spectrum [*Adams*, 1975] and, by an unfortunate quirk of nature, ferric-bearing glasses mimic some of the observed optical behavior of the lunar regolith. However, these experiments   have no relevance to the problem of lunar space weathering.

Vitrification experiments done in vacuo [*Wells and Hapke*, 1993] or in a reducing atmosphere [*Mao et al.*, 1973] show that the only optical effect to be expected from impact melting on the lunar surface is the deepening and broadening of absorption bands. Thus this process is unable to account for the major spectral changes caused by space weathering.

A further argument against the vitrification hypothesis is the following. *Pieters et al.* [1993] measured the spectra of size separates of lunar soil samples. As described in section 3, the fraction < 10 μm in size has optical properties that are distinctly different from the other sizes. However, when larger size fractions were ground to < 10 μm, the resulting spectrum was different from the smallest size fraction. If the space weathering effects were caused by glass, the spectra would be expected to be similar. The fact that the spectra are different is consistent with the space weathering effects being concentrated in the surfaces of the grains, rather than in their volumes, as would be expected if the vitrification hypothesis were correct.

4.3. Simulated Solar Wind Irradiation Experiments

4.3.1. Introduction. The solar wind hits the surface of the Moon during most of its orbit unimpeded by magnetic fields or atmospheres. It consists of a plasma of solar composition streaming outward supersonically from the Sun at speeds of about 500 km s^{-1} [Brandt, 1970], corresponding to a flux of 1×10^8 H$^+$ ions - cm^{-2} s^{-1} with energies of about 1 kev, plus a similar flux of 50 eV electrons, and smaller numbers of He^{2+} and heavier ions. The fluxes and energies increase during periods when the Sun is active. The various types of experiments that were carried out to study effects that this irradiation might have on the optical properties of the lunar regolith are described in this section.

4.3.2. Irradiation of solid surfaces. Shortly after the discovery of the solar wind, *Wehner* [1961] suggested that the surfaces of bodies exposed to it might be reduced to free metal by simple chemical reduction of metal oxides by solar wind H atoms implanted into the mineral surfaces. Several groups subsequently investigated this suggestion by irradiating silicate rocks and minerals with H ions in the laboratory.

Wehner et al. [1963] measured sputtering yields for several metals and silicate rocks with incident H ions of kilovolt energies, and found values ~ 0.01 atoms ion^{-1}. *Hapke* [1966, 1973] irradiated slices of a variety of igneous rocks and minerals with 1.5 keV H ions. *Dybwad* [1971] irradiated flat single crystals of several minerals with 5 kev H ions. *KenKnight et al.* [1967] bombarded flat-surfaced targets of unspecified composition [but presumably silicates] with 0.5 keV H ions. *Housley and Grant* [1977] sputtered a flat slab of synthetic glass of the same composition as Apollo 11 basalt with 1 keV Ar ions. None of these papers reported darkening or any other sign of free metal on the sample surfaces. Housley and Grant analyzed their sputtered surface using X-ray photoelectron spectroscopy [XPS] and did not detect any evidence for the reduction of Fe^{2+} to Fe^0.

The most recent attempt to induce changes by irradiating a solid surface was by *Dukes et al.* [1999], who bombarded olivine with 1 keV H and 4 keV He ions to doses of up to 1×10^{18} ions cm^{-2}. Although subsequent XPS analysis found extremely minor amounts of reduced iron on the irradiated surfaces, there was no visible change in the appearance of the olivine.

The result of all these experiments is consistently negative. When a nonporous, solid surface is bombarded by H ions, no darkening or reddening occurs. The *Dukes et al.* [1999] experiment shows that while a tiny amount of free metal might be produced, it is nowhere near sufficient to affect the optical properties. See also section 5.3.

4.3.3. Hydrogen ion irradiation of loose powders. Several groups bombarded loose, porous powders of a variety of compositions with ions. All workers observed pronounced spectral darkening and reddening.

Wehner and his colleagues [*Wehner*, 1964; *Rosenberg and Wehner*, 1964; *KenKnight et al.*, 1967] used a H gas discharge to irradiate pulverized samples of a variety of terrestrial silicate rocks and also a meteorite. Ions and electrons of mean energy 0.5 keV were alternately extracted by placing the powder on an electrode whose voltage was varied between ±800 V at a frequency of 48 MHz. The samples all darkened and reddened.

Hapke [1965, 1966, 1968, 1973] and *Hapke et al.* [1970] irradiated a wide variety of powders in two different vacuum systems. One system was evacuated by an oil diffusion pump; the other was an oil-free, organic-free, all-metal system evacuated by a getter - ion main pump and roughed by a sorption pump. In both systems the ion gun consisted of a gas discharge held at 2 kV above ground, with ions being extracted through a grid. The ion beam was current-neutralized by flooding the target with electrons from a tungsten filament at a potential a few volts above ground. The temperatures of the targets did not exceed 300° C, well below their melting temperatures. The target powders included pure oxides, silicate minerals, terrestrial igneous rocks, lunar rocks, and meteorites.

Table 1. Effects of Hydrogen Ion Irradiation on Albedo[a]

| Material	Particle Size, μm	Normal Albedo (550nm) Unirradiated	Irradiated
Oxides			
SiO$_2$	< 10	0.58	0.58
Al$_2$O$_3$	< 10	0.77	0.78
MgO	< 10	0.96	0.87
Minerals			
Bronzite	< 7	0.52	0.12
Terrestrial Rocks			
Rhyolite	< 7	0.53	0 18
Basalt	< 7	0.45	0.06
Lunar Rocks			
Apollo 10022	< 37	0.18	0.12
Meteorites			
Bonita Springs (H5)	< 20	0.12	0.03
Colby (L6)	< 20	0.17	0.03
Forest City (H5)	< 20	0 16	0.04
Holbrook (L6)	< 20	0.17	0.04
Indarch (E4)	< 20	0.08	0 03
Murray (CM2)	< 20	0.07	0.03
Plainview (H5)	< 20	0.14	0.04

[a]Data from *Hapke* [1966, 1968, 1973]
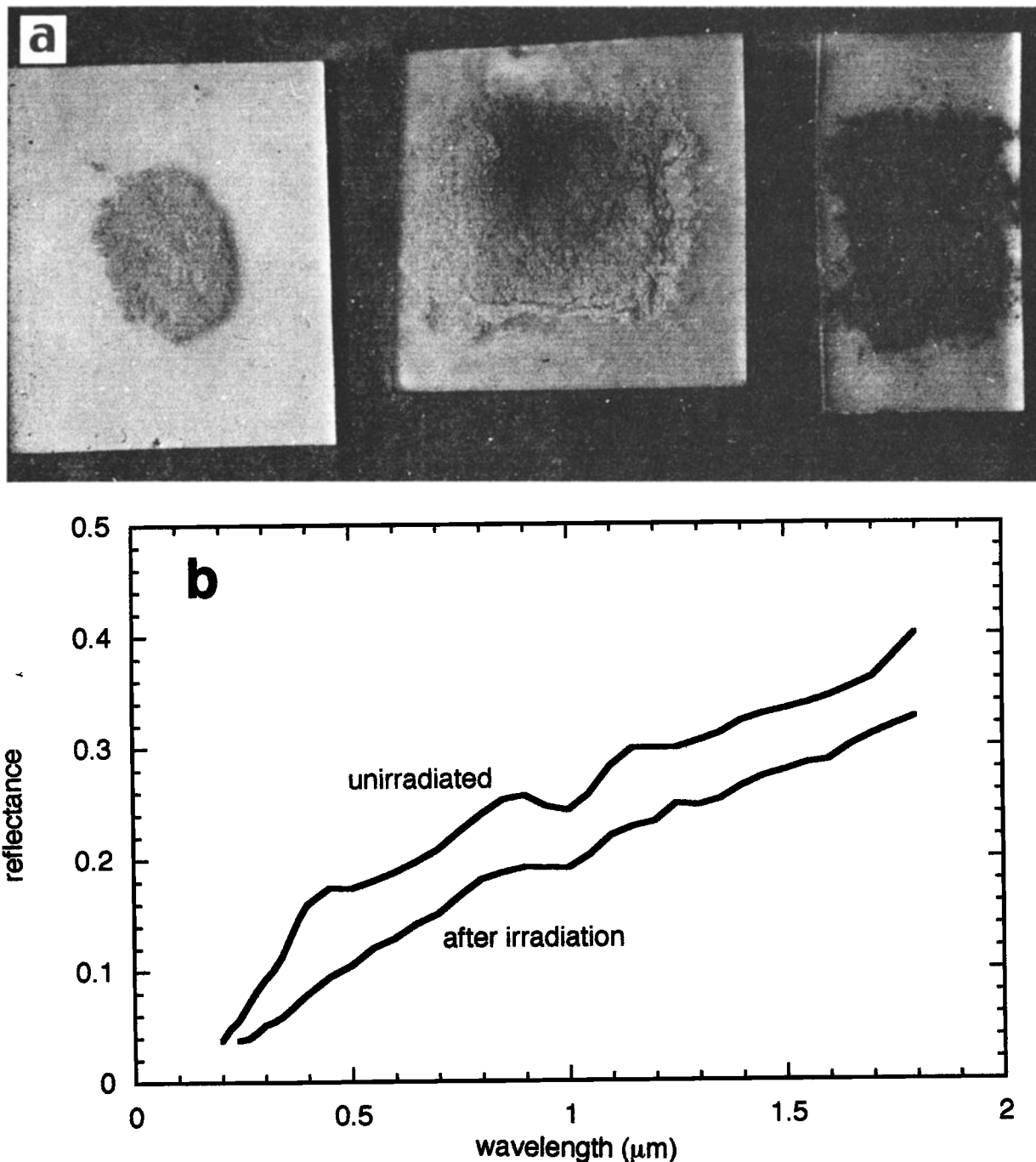
Figure 7. Effects of a simulated solar wind of 2 keV H ions on silicate powders. (a) From left to right: unirradiated pulverized lunar rock 10022; irradiated powdered rock; and lunar soil 10084. (b) Spectra of the unirradiated and irradiated 10022 powdered rock shown in Figure 7a. (c) Powdered terrestrial rocks and minerals before (top images) and after (bottom images) H - ion irradiation. Figure 7c is reproduced from *Hapke* [1966] with the kind permission of the Johns Hopkins University Press.

The compositions of the powder samples and the changes in albedos caused by the irradiation are listed in Table 1. Figure 7 illustrates the changes in spectra and appearance induced by the irradiation. With two exceptions, all powders darkened and reddened. A strong correlation was noted between amount of darkening and Fe content, with high-Fe materials darkening much more than low-Fe ones. The samples that did not darken were ultrapure iron-free SiO_2 and Al_2O_3.

Both Wehner and his coworkers and Hapke and his colleagues found that the changes in optical properties saturated after the targets received a total dose of about 30 C cm^{-2}, which corresponds to a time of about 100,000 years on the lunar surface.

4.3.4. Inert gas ion irradiation of loose powders. *Hapke* [1966] irradiated several materials with He ions and observed pronounced darkening in powdered targets containing Fe. *Yin*
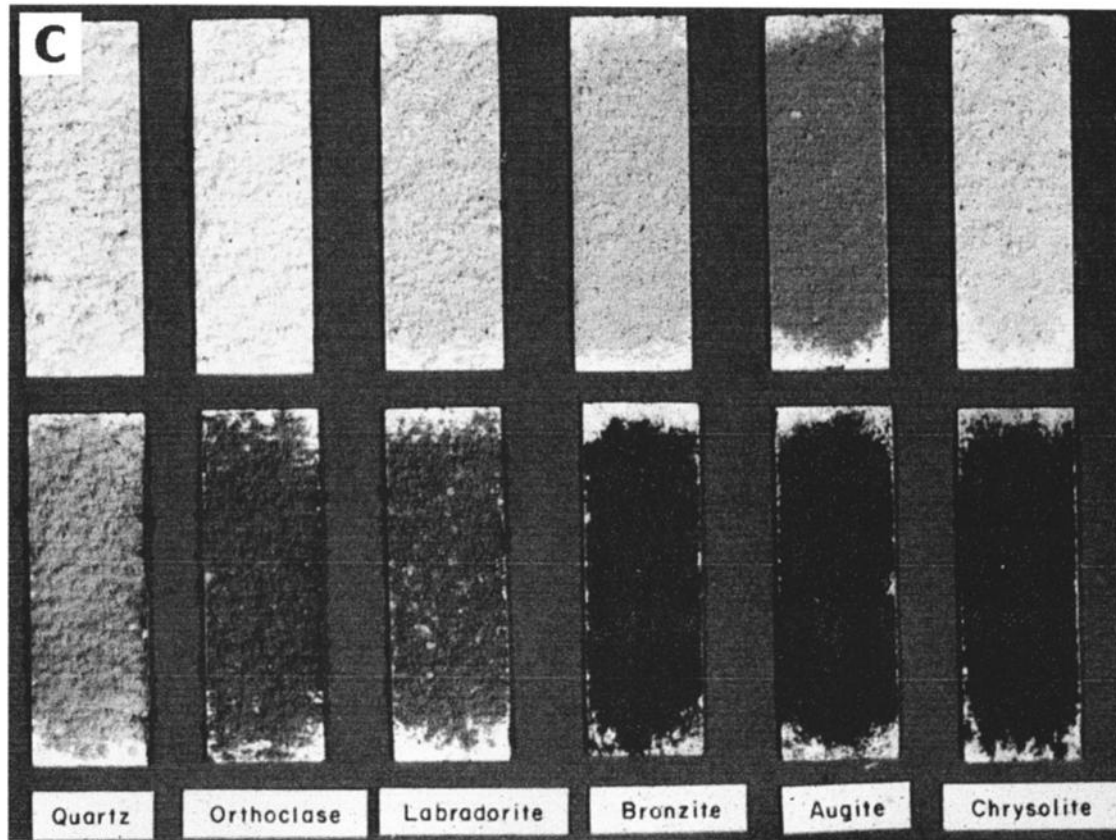
Figure 7. (continued)

et al. [1972, 1975] and *Yin and Tsang* [1976] irradiated a variety of powders, including oxides and silicates, with 1.5 keV Ar ions and found that minerals containing Fe darkened. These experiments show that the ions need not be reducing in order to lower the albedos of the powdered targets. Thus the darkening is not due to simple chemical reduction of Fe^{2+} to Fe^0 by the incident ions.

4.3.5. Importance of a rough, porous texture for sputter darkening. The experiments summarized in this section showed that loose powders irradiated with kilovolt ions will
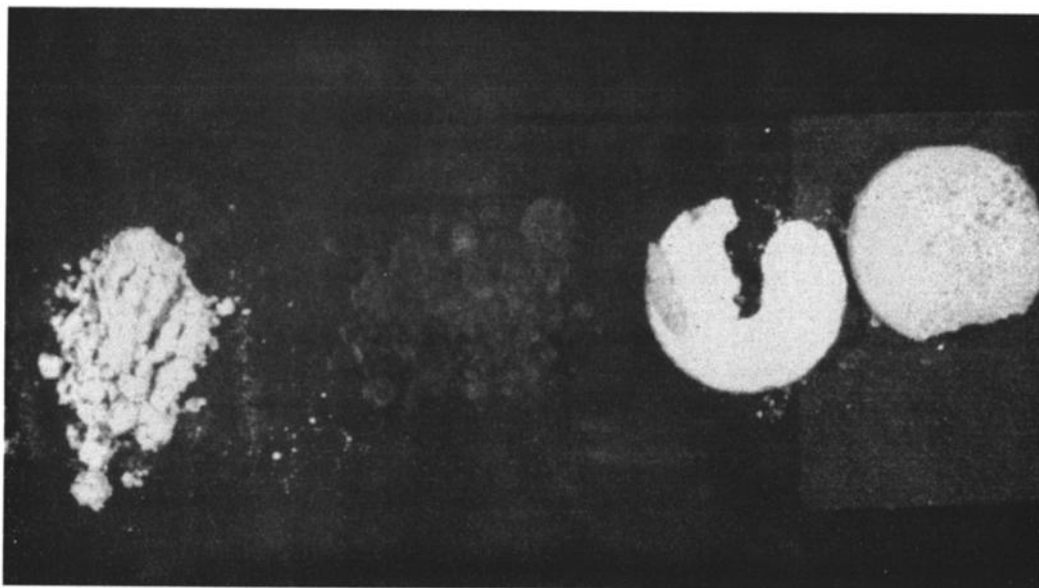

Figure 8. The importance of surface structure for sputter darkening. The material is terrestrial andesite powder. From left to right: unirradiated loose powder; irradiated loose powder; unirradiated powder compacted in a pellet press; and powder irradiated after compaction in a pellet press. Reproduced from *Hapke* [1973] with the kind permission of Kluwer Academic Publishers.
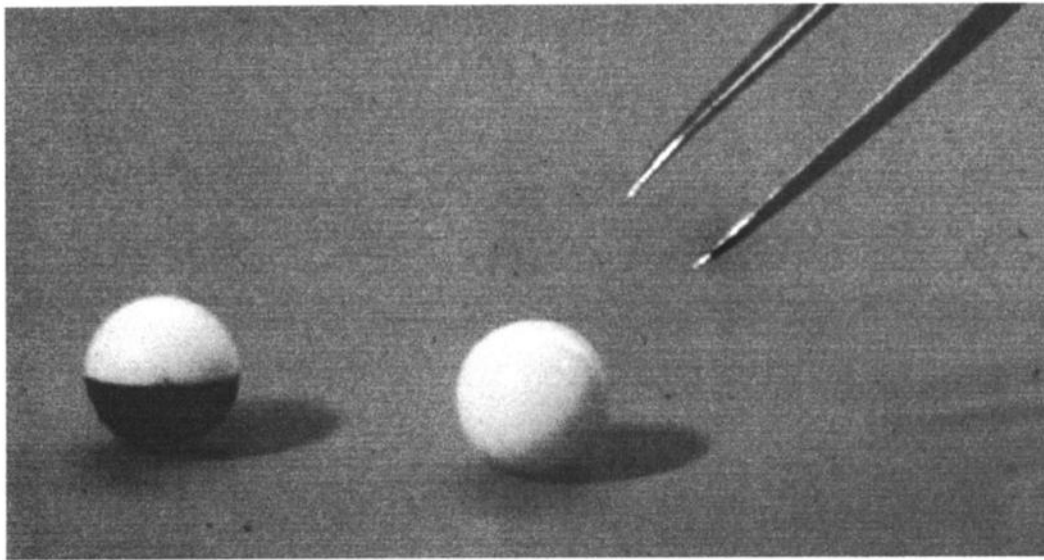
Figure 9. Sputter - deposited coating on the bottom of a ball of alumina. The left ball was irradiated by H ions while on the bottom of an alumina crucible. The right ball is unirradiated. Reproduced from *Hapke* [1966] with the kind permission of the Johns Hopkins University Press.

darken and redden, while flat, smooth samples show little or no change in optical properties. *Hapke* [1966] irradiated a few samples of scoria and pumice and found that they also darkened somewhat, but not nearly as much as when in powder form. Hence the texture of the surface is extremely important in similated solar wind bombardment experiments.

Figure 8 demonstrates the importance of a porous target structure. A loose powder of terrestrial andesite was irradiated alongside a sample of the same powder compressed in a pellet press. The loose powdered sample darkened, while the top of the pressed pellet remained light.

The reason only loose powders darken becomes clear upon examining figure 9, which shows the result of H ion irradiation of a ceramic ball of impure alumina resting on the bottom of an alumina crucible. The top of the ball where the ion beam hit remained light, but the underside darkened. Clearly, atoms sputtered from the inside of the crucible coated the underside of the ball with an absorbing film that was shielded from the ion beam by the top of the ball. It is the deposits of sputtered atoms that are dark, rather than the directly sputtered surfaces.

Instead of irradiating a powder, a lunar rock was placed next to a fused SiO_2 slide and bombarded with H ions [*Hapke et al.*, 1975a]. The slide was shielded from the beam, but could see the target and thus collect sputtered material. The
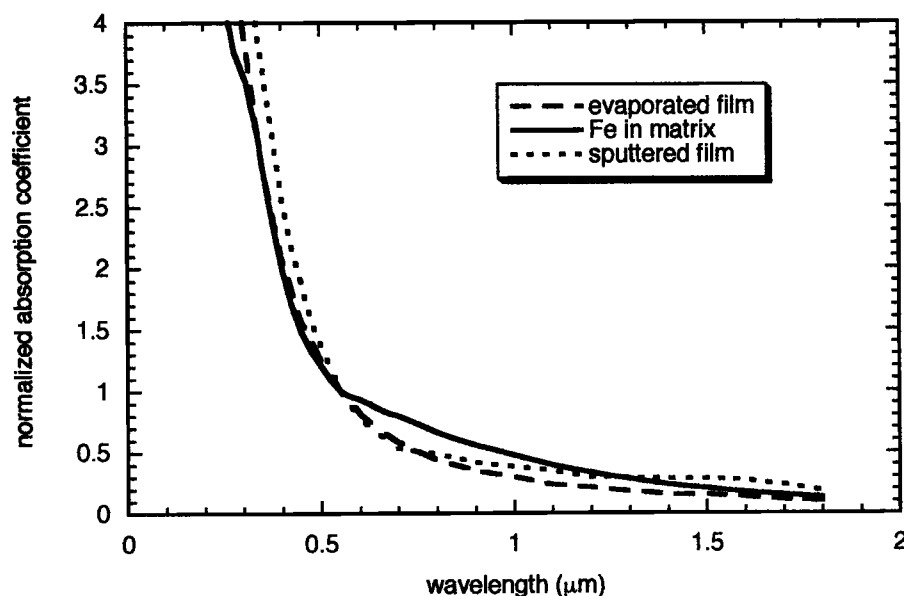

Figure 10. Absorbance spectra of films containing submicroscopic metallic iron (SMFe): Film sputtered from lunar rock 10017 (dotted line); film evaporated from rock 10017 (dashed line); and theoretical absorption coefficient of SMFe in a nonabsorbing matrix (solid line). The curves have been normalized at 550 nm.

transmission spectrum of the sputter-deposited film from a lunar rock is shown in Figure 10. The film is strongly absorbing and has a lower transmission in the red than in the blue so that it appears brownish in color. The film spectrum has no absorption bands. These are just the properties required to cause the optical space weathering effects in the lunar regolith.

When a flat, smooth surface is irradiated, all of the sputtered atoms are lost from the target. However, when the target is a porous powder, two effects allow the powder to retain most of the sputtered atoms. First, many of the incident ions pass between the particles in the top layer and sputter material from the particles in lower layers. Most of this sputtered material coats the undersides of particles in the upper layers. Second, atoms sputtered by the ions that are incident at glancing angles onto the sloping sides of particles tend to preserve the momentum of the incident ions [*Wehner*, 1959] and are sputtered preferentially downward into the powder, where they coat the underlying particles. If the target is undisturbed, the upper layer of particles will eventually be welded together by the sputtered films to form a dark, coherent crust [*Wehner*, 1964]; however, on the surface of the Moon such a crust is disaggregated by micrometeorite impacts before it can develop.

Even though the films coat only the sides and bottoms of particles, the powder is still darkened. The reason is that most of the light scattered by the powder is refracted and transmitted all the way through one or more particles and partially absorbed by the coatings before being scattered by other particles and emerging from the powder. Light reflected from the upper surfaces of the top layer of grains contributes only a minor amount to the total light scattered by the powder.

4.3.6. Importance of current neutralization when irradiating insulators: The experiments of Nash. *Nash* [1967] attempted to study sputter - darkening by irradiating samples with 5 keV H ions. However, his results were inconsistent: Sometimes his samples darkened and sometimes not. Often when darkening occurred, it was not confined to the samples, but spilled over onto adjacent areas. He suggested that contamination was the reason his samples darkened and that the darkening observed by other workers might also be spurious, thus casting doubt on the sputter - darkening hypothesis.

In response, the author carried out a large number of irradiations of many substances under a variety of carefully controlled conditions; detailed descriptions of these experiments can be found in the work by *Hapke* [1973]. The results virtually eliminated the possibility that the darkening observed by him was spurious. Among the strongest arguments is the fact that only Fe-bearing materials, such as bronzite, darkened, even when irradiated side - by - side with Fe-free SiO$_2$, which remained light.

Again, over 30 years after the fact, one can only speculate. However, in retrospect, the reason for the discrepancies seems clear. The ion beam was not current-neutralized in most of Nash's experiments. However, it is essential that this be done when irradiating insulating targets. If not, the surface of the target will charge up until it repels or deflects the ions so that

they hit electrodes or other grounded metallic surfaces and sputter material from these structures. The sputtered material will coat everything, as was observed in Nash's experiments. In a few of his later irradiations the beam was current-neutralized. In some of these, the targets were pressed powders and did not darken. However, on the basis of the discussion of section 4.3.5, the lack of darkening of pressed powders is to be expected. Nash did irradiate a few loose, porous powders with a current-neutralized ion beam and found they, in fact, darkened by the same amount as observed by other experimenters. Hence instead of refuting sputter - darkening, a strong case can be made that Nash's results actually support it.

4.3.7. Summary of the ion irradiation experiments. (1) In several independent experiments in which Fe-bearing powders were irradiated with a simulated solar wind, spectral darkening and reddening were observed. (2) The target material must contain Fe in order for darkening to occur. (3) Only loosely packed powders darken; pressed powders and solid targets with flat surfaces remain light. (4) H ions are not necessary to produce darkening; sputtering by inert gas ions also darkens powders. (5) The darkening is caused by thin coatings of sputtered material deposited on the sides and bottoms of grains; the directly sputtered surfaces remain light. (6) The apparent contamination darkening observed by one worker is readily explainable as caused by failure to current - neutralize the ion beam in his experiments.

4.4. Evaporation Experiments

The ion irradiation experiments described in section 4.3 show that films of atoms deposited by sputtering will darken an Fe-bearing powder. In addition to sputtering, films of silicate vapor can also be deposited on the surfaces of airless bodies by meteorite impacts. Consequently, *Hapke et al.* [1975a] and *Cassidy and Hapke* [1975] investigated the optical properties of condensates produced by evaporating lunar and terrestrial silicates in vacuum. Initially, the vaporizations were done in two ways: by coating a bare tungsten filament with powdered rock and discharging a capacitor through the filament, and by placing powder on an electrically heated graphite strip. Some of the resulting vapors were condensed on nearby slides of fused SiO$_2$. The condensates were found to be strongly absorbing and brownish, similar to the sputter-deposited films.

However, there was concern about the possibility of contamination by the tungsten or carbon heaters, so two vaporization methods which were free of such contamination were tried. The first method was flash-heating of a lunar rock in vacuum by bursts of IR radiation from a pulsed high-power laser. This is probably the closest laboratory simulation of impact vaporization on the lunar surface, short of actually carrying out a hypervelocity impact experiment. Brownish deposits of vapor on a fused SiO$_2$ slide were observed. Unfortunately, with the experimental set-up available to the authors at that time it was not possible to produce enough film in this way to reliably measure its properties.
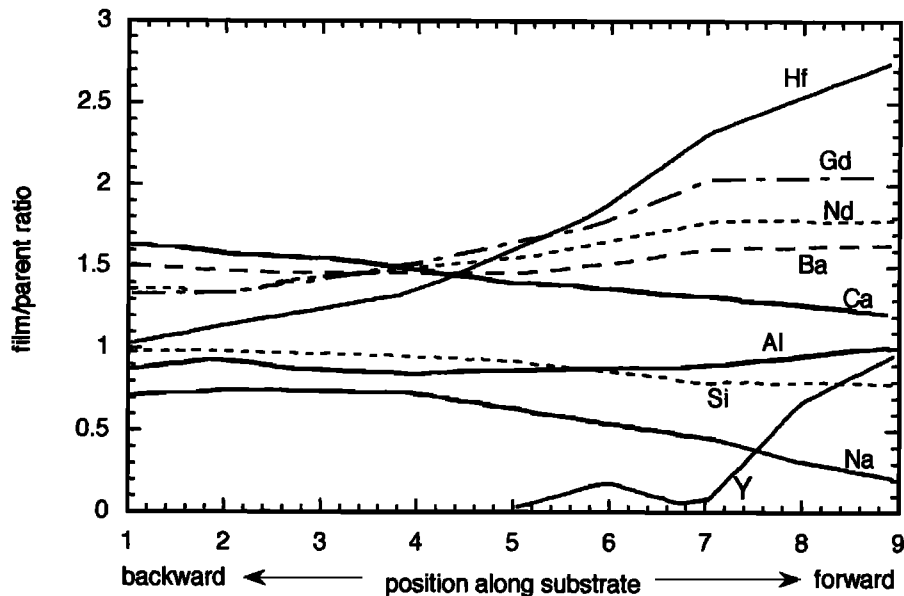
Figure 11. Effect of angle on composition of a sputter-deposited film. The sputter target was an artificial glass whose surface was oriented 45° from the direction of the incident ion beam. The substrate on which the film was deposited was a Mo foil, which was shielded from the ion beam, but could see the target glass. Points on the right-hand side of the substrate collected atoms that were predominantly sputtered in a forward direction, and points on the left were predominantly sputtered backward. The target glass and film were analyzed by electron microprobe. The figure shows the ratios of abundances of atoms in the film to those in the parent at several points along the film [*Paruso et al.*, 1978]. Heavier atoms like Hf and Gd were preferentially sputtered in the forward direction, while lighter atoms like Na and Ca were preferentially sputtered backward.

The most satisfactory vaporization technique used an electron beam furnace (e-gun) operating in a high vacuum. In this apparatus, electrons are emitted from a tungsten filament that is shielded from the sample and held at a high negative voltage. The electron beam is magnetically bent and focused onto the sample, which rests on a grounded, water-cooled copper block. Temperatures well over 2000° C, as measured by an optical pyrometer, are readily obtainable. Since only the
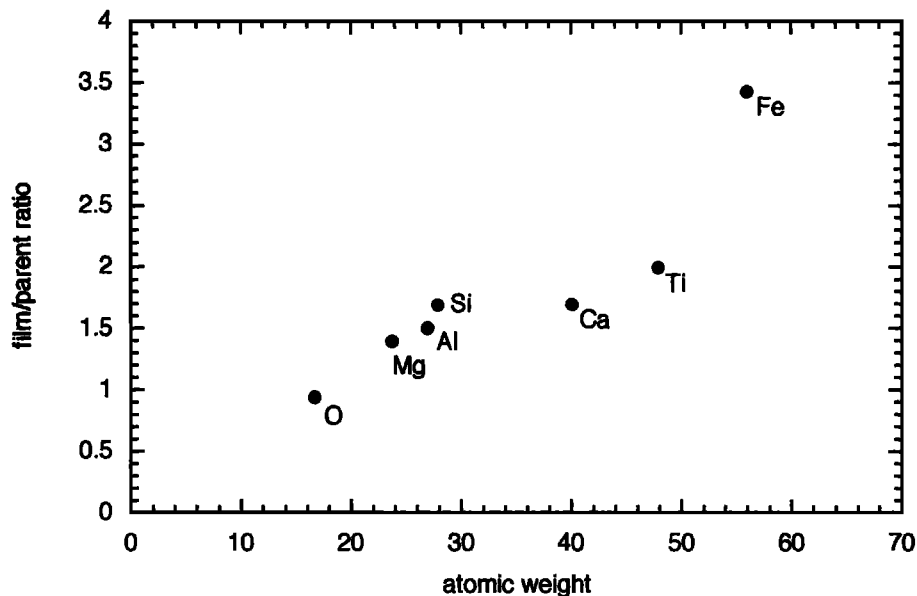

Figure 12. Effect of atomic weight on composition of a sputter-deposited film. The sputter target was an artificial glass, whose composition was the same as the major elements in Apollo 11 rocks, and whose surface was oriented at 45° from the ion beam. The substrate was a Mo foil positioned to receive atoms sputtered in the forward direction. The figure shows the ratios of abundances, as analyzed by electron microprobe, of atoms in the film to those in the sputter target plotted against atomic weight. The film is enriched in heavier atoms. Reproduced from *Hapke et al.* [1975a] with the kind permission of Kluwer Academic Publishers.

target material is heated, there is no possibility of contamination by a crucible. Both lunar and terrestrial rocks were evaporated using the e-gun. Again, the resulting condensates were strongly absorbing and brownish in color. Under an optical microscope the films appeared clear and amorphous.

A transmission spectrum of a typical condensate is shown in Figure 10 and is seen to be very similar to that of the sputter-deposited film. Thus the optical properties of vapor deposits do not depend strongly on how the vapor is generated.

Moroz et al. [1996] and *Yamada et al.* [1999] irradiated powdered terrestrial minerals with short bursts from a high powered laser and observed spectral darkening and reddening. Moroz et al also irradiated pulverized meteorites with similar results. They interpreted the spectral changes as resulting from impact vitrification. However, as discussed in this and the preceding section, this interpretation is very probably incorrect. It is highly likely that the optical changes resulted from deposits of vapor generated by the laser shots.

4.5. Chemical Fractionation During Vapor Transport

Several effects might be expected to cause differences in composition between sputtered or evaporated coatings and their parent materials:

1. Different atomic species in a multicomponent ion-bombarded target have different sputtering yields. However, this is a very minor effect. It results in the creation of a transition layer only a few nanometers thick on the target surface in which the high-yield species are depleted. Once this layer is established, sputtering is stoichiometric [*Tarng and Wehner*, 1971; *Hapke and Cassidy*, 1978]. The

sputtering experiments on flat surfaces show that this layer is too thin to have any effect on the optical properties of the target.

2. If the ion beam is not incident vertically on the target surface, the sputtering yield is anisotropic, with high mass atoms preferentially forward sputtered and low mass atoms preferentially back sputtered [*Paruso et al.*, 1978]. This is illustrated in Figure 11, which shows the change in composition of a sputter-deposited film with sputtering angle. Figure 12 shows the composition of a sputtered film relative to the target plotted against atomic weight. The ion beam was incident on the target at an angle of about 45° from the normal to the target surface, and the film was collected at a similar angle in the forward - sputtering direction. Note the positive correlation between enrichment ratio and atomic weight. Iron, the heaviest major element in the sputter target, is the most enriched, while oxygen, the lightest element, is depleted relative to the cations in the film.

Because atoms sputtered in the backward direction tend to be preferentially lighter than those in the forward direction, sputter-deposited films on the surfaces of lunar regolith grains could be either enriched or depleted in heavier atoms and isotopes, depending on their location relative to the surfaces being directly sputtered by the solar wind. However, the back - sputtered atoms are more likely to escape from the regolith, so that lunar sputter deposits are probably preferentially enriched in atoms and isotopes of higher atomic weight.

3. During thermal vaporization the more volatile species are preferentially evaporated. Thus, impact condensate flims in a regolith would be expected to be enriched in the more volatile elements [*Hapke et al.*, 1975a]. Figure 13 shows the film/parent enrichment ratio for a film condensed from a rock evaporated at 1900° C plotted against vapor pressure of the
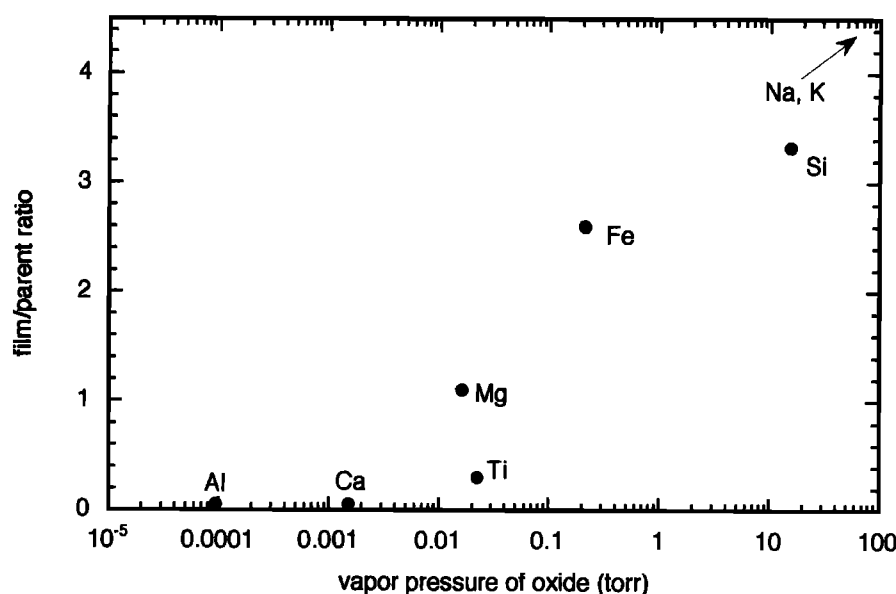

Figure 13. Effect of vapor pressure on composition of an evaporation - deposited film. The parent material was an artificial glass, whose composition was the same as the major elements in Apollo 11 rocks, heated to 1900° C in an electron beam furnace in vacuo. The substrate was a Mo foil. The figure shows the ratios of abundances, as analyzed by electron microprobe, of atoms in the film to those in the parent glass plotted against the vapor pressure at the evaporation temperature of the metal oxide. The film is enriched in cations whose oxides have the higher vapor pressures. Reproduced from *Hapke et al.* [1975a] with the kind permission of Kluwer Academic Publishers.
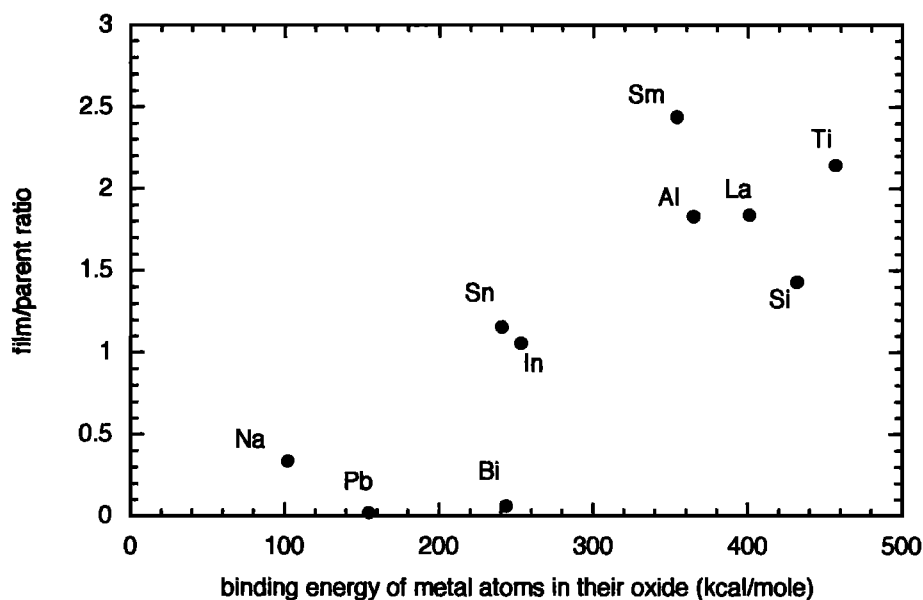
Figure 14. Effect of binding energy on composition of a sputter-deposited film. The sputter target was an artificial glass whose surface was oriented 45° from the direction of the incident ion beam. The substrate on which the film was deposited was a Mo foil, which was shielded from the ion beam, but could see the target glass. The figure shows the ratios of abundances, as analyzed by electron microprobe, of atoms in the film to those in the sputter target plotted against the binding energies of the cations in their oxides [*Paruso et al.*, 1978]. The film is enriched in those cations with higher binding energies.

oxide. Note the positive correlation, and that Fe is one of the more highly enriched elements.

4. Each species present in the vapor has a different probability of being permanently accommodated to the surface on which it is condensing [*Hapke*, 1973; *Hapke et al.*, 1975a; *Cassidy and Hapke*, 1975; *Paruso et al.*, 1978; *Hapke*, 1986]. Initially, the condensing atoms are only weakly physically bound to the surface. During this phase of the condensation process, the atoms are mobile and have a finite probability of desorbing before finding a site where they are strongly chemically bound to the surface. Hence regolith films should be enriched relative to the impinging vapor in elements with high binding energies in their oxides. *Cassidy and Hapke* [1975] called this process "first-bounce fractionation". Figure 14 shows the positive correlation of the film/parent enrichment ratio with binding energy for a sputter-deposited film.

5. During thermal evaporation the rock-forming oxides are partially dissociated, so that oxygen, free metals and their oxides are all present in the vapor [*DeMaria et al.*, 1971], and each has a different sticking probability. Specifically, since O is the most volatile species in a silicate vapor, it has the lowest sticking probability and highest desorption probability.

All of these fractionation processes tend to leave the films depleted in oxygen and enriched in Fe. The missing oxygen will be compensated by the reduction of the major oxide with the lowest binding energy, which in most mafic silicates is FeO. *Hapke et al.* [1975a] suggested that this was the source of the SMFe in both the sputtered and thermally evaporated films, and that the SMFe was the cause of the large absorption coefficient and also the ESR resonance [see sections 5.7 and 5.8] displayed by the films. They further suggested that SMFe-

rich vapor-deposited coatings on and in grains of lunar soil are the cause of lunar space weathering.

5. Lunar Sample Analyses and Experiments

5.1. Introduction

In this section several different types of measurements on lunar samples and laboratory analogs that support the hypothesis of SMFe-rich coatings on lunar regolith grains are described. These include acid leaching, Auger and X-ray electron spectroscopy, magnetic, electron spin resonance and transmission electron microscope studies.

5.2. Acid Leaching

Gold et al. [1970] and *Hapke et al.* [1970] treated samples of lunar soil with a solution of 20% hydrochloric acid. After only a short exposure to the reagent, the albedo increased, the spectrum became less red, and the depth of the absorption bands increased (Figure 15). Thus the lunar darkening agent is in locations on or close to the soil grain surfaces where it is readily accessible to the acid.

5.3. Grain Surface Analyses

Auger electron spectroscopy (AES) and/or X-ray photoelectron spectroscopy (XPS) studies of lunar samples were carried out by several workers [*Vinogradov et al.*, 1972; *Gold et al.*, 1974, 1975, 1976; *Housley and Grant*, 1975, 1976, 1977; *Baron et al.*, 1977, 1978; and *Dikov et al.*, 1978]. These analytical techniques are sensitive to only the outer few monolayers of atoms on the surface being analyzed.
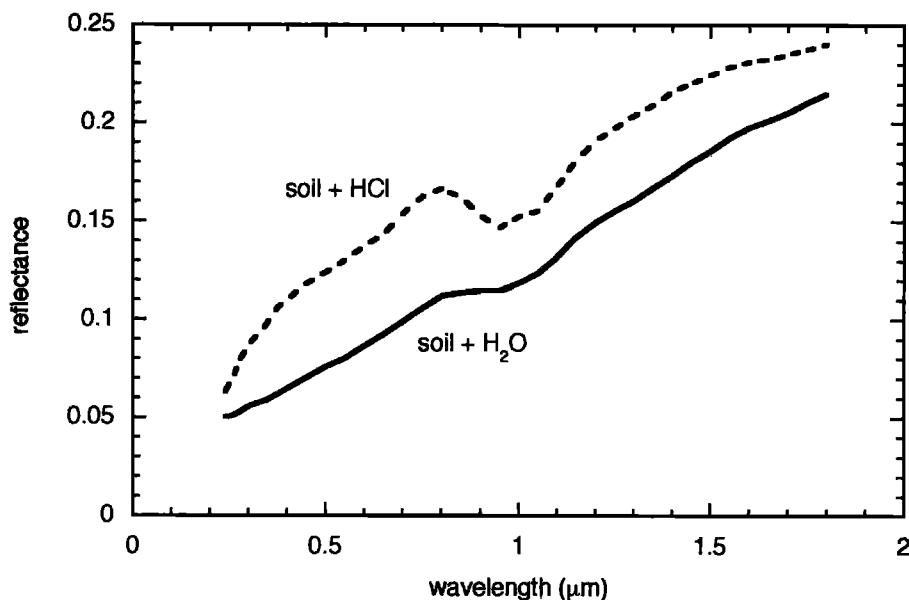
Figure 15. Bidirectional reflectance spectra ($i = e = 30°$, $g = 60°$, relative to a MgO standard) of lunar soil 10084 after soaking in distilled water and in a solution of 20% HCl for 2 hours. The leaching changed the spectrum so that it more closely resembled that of an Apollo 11 rock.

Using XPS, *Vinogradov et al.* [1972] discovered that part of the iron is reduced on the surfaces of the grains. They estimated that 10 - 15% of the surficial Fe is in reduced form.

In the work by Gold et al., Housley and Grant, and Baron et al., spectra were obtained of fine grain separates from several lunar soil samples and compared with spectra of crushed coarse grain separates from the same samples. It was assumed that the surfaces of the crushed coarse grains were representative of the interiors of the lunar soil particles. Gold et al. and Baron et al. found that Fe was increased on the surfaces of the grains as compared to the interiors by as much as a factor of 2, while Housley and Grant found little or no enrichment. Both sets of

workers discussed the discrepancy at length and could find no obvious reason. However, Baron et al. [1978] pointed out that a major difference between the experiments is that Gold et al. and Baron et al. measured pristine soil samples, while Housley and Grant prepared their samples by sedimenting them onto the holders in ethanol followed by a bake out in vacuum at 300° C. The effect this treatment may have had on the soil grain surfaces is unclear.

However, all parties agreed that reduced Fe is present on the surfaces of lunar soil grains, but not in their interiors, nor is it present in the interiors of the lunar rock samples (Figure 16). Using ion milling, *Housley and Grant* [1977] found that
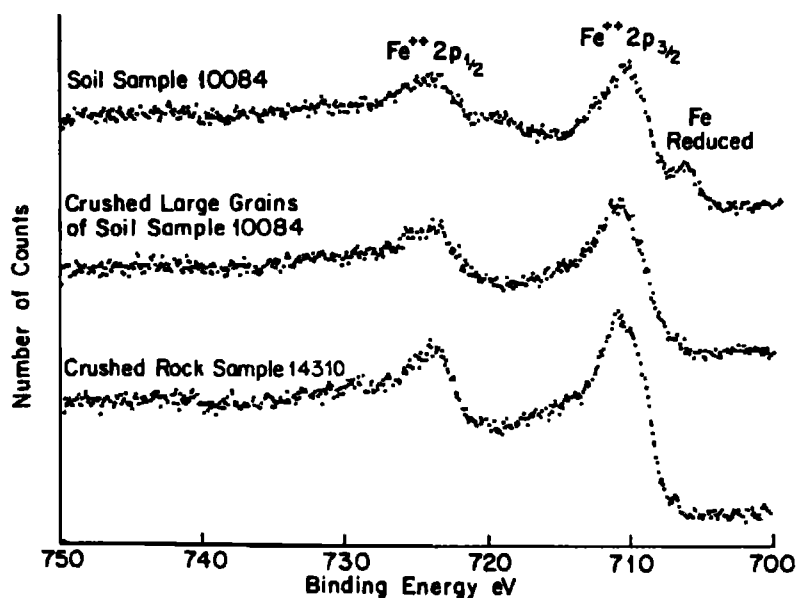

Figure 16. X-ray photoelectron spectra of a pristine sample of lunar soil 10084, crushed large grains separated from 10084, and crushed lunar rock 14310. Note the peak indicating surficial Fe^0 in the spectrum of the pristine soil. Reproduced from *Baron et al.* [1977] with the kind permission of Elsevier Science.

as much as 25% of the Fe was in the form of Fe^0 in a surface layer about 25 nm thick.

Dikov et al. [1978] studied lunar soil by XPS and found that not only Fe, but also Ti, Si and Al are partially reduced. However, other XPS workers did not report that any other elements besides Fe are reduced, even though their measurements were capable of detecting them. The reason for this discrepancy is unclear at present. On the other hand, *Hapke* [1977] found that condensates of evaporated Fe-free powders showed some absorption in the blue and UV that could have been produced by Si and Al metal.

Dikov et al. used ion milling along with XPS to profile the valence state with depth of several elements in the soil. They showed that the reduced elements are confined to a surface layer several tens of nanometers thick, and that the reduced fraction decreases monotonically with depth. These authors interpreted their profiles as describing the actual distribution of metal atoms with depth and as implying that the reduction was by direct action of the solar wind hydrogen. However, in view of the discussion in section 4.3.2, this interpretation is questionable. The XPS measurements by *Dukes et al.* [1999] on olivine, described in section 4.3.2, show that irradiation of a solid surface by H and He ions causes negligible reduction. Dikov et al. measured a large number of lunar soil grains simultaneously; thus a more likely interpretation is that the metal is located in vapor-deposited coatings of variable thickness and that the profiles describe the statistical distribution of the thicknesses.

Yin et al. [1972, 1975] and *Yin and Tsang* [1976] used XPS to analyze the surfaces of terrestrial mineral powders that they had irradiated with 1.5 keV Ar ions. Only the powders composed of Fe-bearing minerals, such as fayalite Fe_2SiO_4, were darkened by the irradiation, and it was found that some of the Fe^{2+} had been reduced to Fe^0 on the grain surfaces.

5.4. Magnetically Separated Soil Fractions

If a soil sample is separated into magnetic and nonmagnetic components, the magnetic component is much darker (Figure 17). This shows that the darkening agent is associated with a ferromagnetic phase in the soil.

5.5. Measurements of Magnetization

Magnetization curves of several materials were measured up to fields of 1.6 T [*Cassidy and Hapke*, 1975; *Hapke et al.*, 1975a]. The high-field susceptibility depends on the amounts of both paramagnetic iron (as FeO) and superparamagnetic iron (in the form of metallic Fe of grain size smaller than about 8 nm). The remanent magnetization depends on the amount of metallic Fe in larger grain sizes [single domain and multidomain Fe]. A synthetic glass of the same composition as Apollo 11 basalt had a magnetization curve consistent with 12.3% paramagnetic FeO and negligible metallic Fe, in reasonable agreement with the 15% FeO originally added to the glass. A condensate made from evaporating this glass in vacuo at 1900° C had a magnetization curve consistent with about 10% by weight of superparamagnetic Fe, but negligible metallic Fe in larger grain sizes. The film was then rapidly heated to 800° C and immediately cooled, the whole thermal cycling process taking about 1 min. This flash - annealing changed the magnetization curve in a manner consistent with a decrease in the amount of superparamagnetic Fe and an increase in the single domain and multidomain Fe to 11%. Evidently the smaller Fe particles rapidly diffused through the medium during the flash - annealing and coalesced into larger sizes.

Similar measurements attempted on sputter-deposited films were of low precision because of the small sample size. However, the magnetization curve of the unannealed film was consistent with a superparamagnetic Fe content greater than 1%.
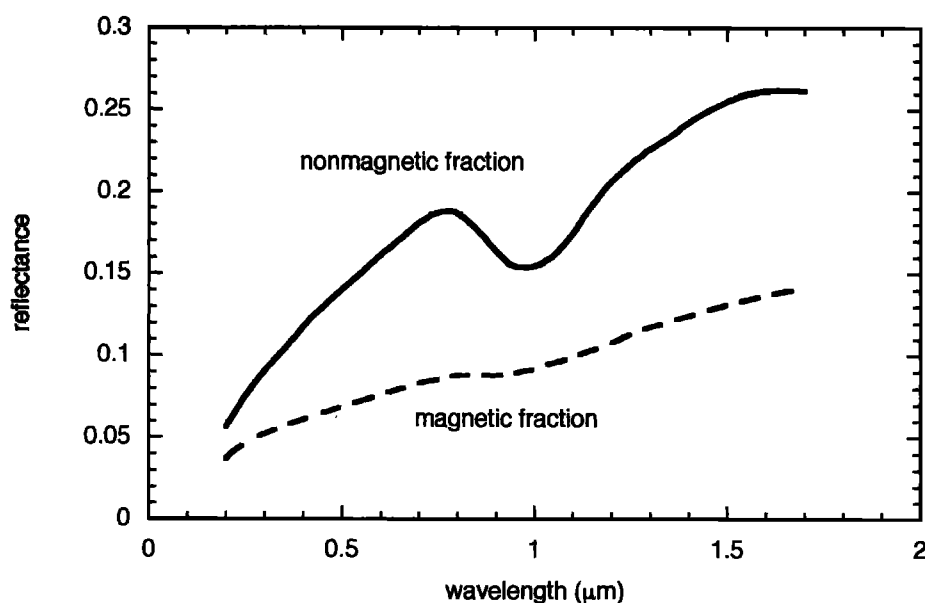

Figure 17. Bidirectional reflectance spectra ($i = e = 30°$, $g = 60°$, relative to a MgO standard) of the separated magnetic and nonmagnetic fractions of lunar soil 10084.
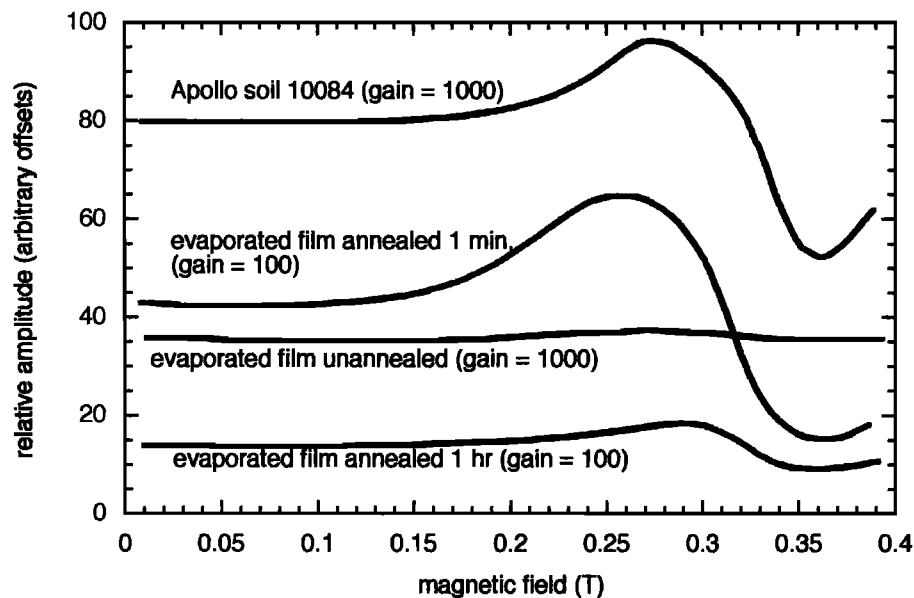
Figure 18. The ferromagnetic resonance spectra of lunar soil 10084 and of a vapor-deposited film evaporated from an artificial glass whose major element composition was the same as an Apollo 11 rock, heated to 1900° C in an electron beam furnace in vacuo. The figure shows the effect on the strength of the resonance of flash annealing and prolonged annealing. Note the different gain settings of the instrument. Reproduced from *Hapke et al.* [1975a] with the kind permission of Kluwer Academic Publishers.

5.6. Electron Spin Resonance Studies of Lunar Soil

The lunar fines have a characteristic electron spin resonance (ESR) at a fine - structure splitting factor of g = 2.1 (Figure 18). Although there was considerable initial debate over the cause of the resonance, there is now general agreement that it is due to metallic Fe particles between about 4 and 33 nm in size in the soil [*Morris et al.*, 1975; *Housley et al.*, 1976; *Morris*, 1976, 1980], and the resonance is now known as the ferromagnetic resonance (FMR). However, the source of the SMFe is still debated.

Morris [1976] has shown that the ratio I_s/FeO of the relative strength of the FMR [denoted by I_s] to the FeO content of a soil sample is a measure of the maturity of the sample; that is, I_s/FeO is a measure of the time the sample has been exposed to the space environment on the lunar surface. The agglutinate content of a soil also increases with maturity. *Housley et al.* [1973] showed that agglutinates are carriers of the FMR, and it is a common misperception that only the agglutinates contain SMFe.

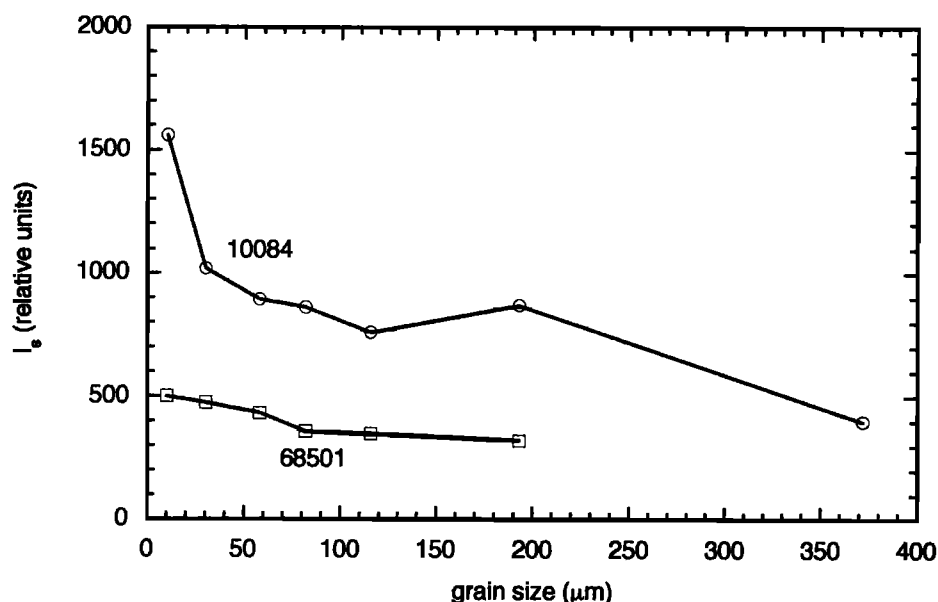*Morris* [1977] showed that I_s increases as particle size

Figure 19. Strength of the ferromagnetic resonance in two samples of mature lunar soil plotted against grain size; 10084 is a mare soil and 68501 is a highland soil (data from *Morris* [1977]).

decreases (Figure 19). This is consistent with the SMFe being located primarily on the surfaces of the grains, rather than being distributed uniformly throughout the interiors of the agglutinates. *Taylor et al.* [1999b] showed that I_s/FeO also increases as size decreases.

Morris [1980] studied the metallic Fe content of a wide range of lunar soils from their magnetization curves and FMR resonances. A typical soil has about 0.54% Fe^0, with highland soils having somewhat smaller amounts than maria regoliths. He estimated that roughly 30% of the Fe is native to the lunar rocks, 30% is meteoritic in origin, and the remaining 40% is the result of reduction of FeO by space weathering. Most of the exposure-reduced Fe^0 is smaller than 33 nm in size, and is responsible for the FMR, while the native and meteoritic Fe^0 particles are larger.

5.7 Electron Spin Resonance Studies of Vapor-Deposited Films

The ESR spectra of several of the films made by evaporation of lunar and synthetic lunar materials were measured at a frequency of 9.11 GHz [*Hapke et al.*, 1975a]. Figure 18 shows a typical result. A synthetic glass of the same composition as Apollo 11 rocks was prepared from pure reagent grade oxides. Some of the glass was evaporated at 1900° C in the e-gun, and the vapor condensed on a fused SiO_2 slide. Figure 18 shows that the unannealed film has a resonance, but that it is rather weak, because most of the Fe particles are in the superparamagnetic size range. However, after flash - annealing to 800° C the size of the resonance increased by a factor of 100 as the Fe particles coalesced and grew into the single domain size range. For comparison, the spectrum of a sample of Apollo 11 soil is also shown and is seen to have a similar resonance. The film was then reheated for 1 hour at 650° C in vacuum, which decreased the resonance by a factor of 10, probably because most of the Fe particles grew to such a size that they were larger than the RF skin depth and were inefficient at exhibiting the resonance. Interestingly, the transmission spectrum of the film was not changed by either of the vacuum annealings, indicating that the light-absorbing agent was not sensitive to Fe particle size, so long as the size was smaller than a wavelength.

5.8. Transmission Electron Microscope Studies

Ever since the Apollo samples became available, it was realized that the soil contains metallic Fe. Some of the Fe is in particle sizes large enough to be seen through an optical microscope [e.g., *Agrell et al.*, 1970]. However, most of the Fe^0 particles are so small that a transmission electron microscope (TEM) is required to image them. *Housley et al.* [1973] used a TEM to study the size distribution of the metallic Fe particles in lunar agglutinates. They estimated that most of the particles there are between about 0.5 and 25 nm in size.

While studying lunar soil samples using TEM, *Borg et al.* [1971] discovered that a large fraction of the grains are covered with films a few hundred nanometers thick, which appeared to be amorphous. Unfortunately, the TEM techniques available at that time were unable to resolve any structure or obtain any

compositional information about the coatings. It was assumed that they were simply the outer portions of the underlying grains that had been metamictized by solar cosmic radiation damage.

However, when Keller and his colleagues [*Keller and McKay*, 1993; 1997; *Wentworth et al.* 1999; *Keller et al.*, 2000; *Pieters et al.*, 2000] utilized improved TEM technology to reexamine the coatings, they discovered that contrary to the earlier assumptions, the rims and patinas have different compositions than the grains they coat. Some of the coatings contain pancakes and blebs that are clearly melt glass, particularly in the glassy rims around microcraters. Many of these are high-Al, Si-poor [HASP] glasses that are believed to be the residues of partially evaporated melt glasses. However, many of the coatings follow the contours of the underlying grain surfaces closely and are of different composition than their host grain; hence they are obviously vapor deposits. Such coatings are ubiquitous on the vast majority of soil grains. Also ubiquitous in the rims are particles of metallic Fe. Although many of the coatings and agglutinitic glasses contain microscopic vesicles, there is no particular spatial association between the Fe^0 particles and the vesicles. A TEM image of a typical rim is shown in Figure 20. The dramatic images published in the papers of Keller and his associates finally provided direct visual proof of the SMFe-rich coatings on the soil grains that had been predicted for so long by the variety of indirect observations described above.

6. The Origin of the SMFe

According to *Morris* [1980] about 60% of the SMFe in the soil is either native Fe that was originally present in the rocks or added by meteoritic impacts. The remaining 40% has been reduced from FeO by exposure to the space environment and is in the form of particles a few tens of nm in size. Several processes that have been proposed to account for this space - reduced SMFe will now be critically assessed.

1. Ferrous ions are reduced by direct chemical interaction with hydrogen implanted by the solar wind [*Wehner*, 1961; *Pillinger et al.*, 1976; *Dikov et al.*, 1978]. This is directly contrary to the results of the many laboratory experiments summarized in section 4.3.2.

2. Impact shock reduces the iron [*Cisowski et al.*, 1973]. This is not supported by laboratory experiments [*Cisowski*, 1976].

3. Baking in a large, impact-generated, thermal blanket reduces the iron [*Pearce et al.*, 1972]. In this hypothesis the chemically reducing conditions are suggested to be supplied by imbedded solar wind H. There are two objections to it. First, there is a serious question as to whether there is enough H in a large thermal blanket. Much of the material in a blanket would have been excavated from well below the surface where it would never have been exposed to the solar wind. Second, it is not enough to just reduce the ferrous iron to metal. The reduction process must leave most of the metallic iron in the form of particles that are small compared to the wavelength. The experiments reported by *Pearce et al.* [1972] and *Allen et al.* [1996b] in which lunar and terrestrial materials were
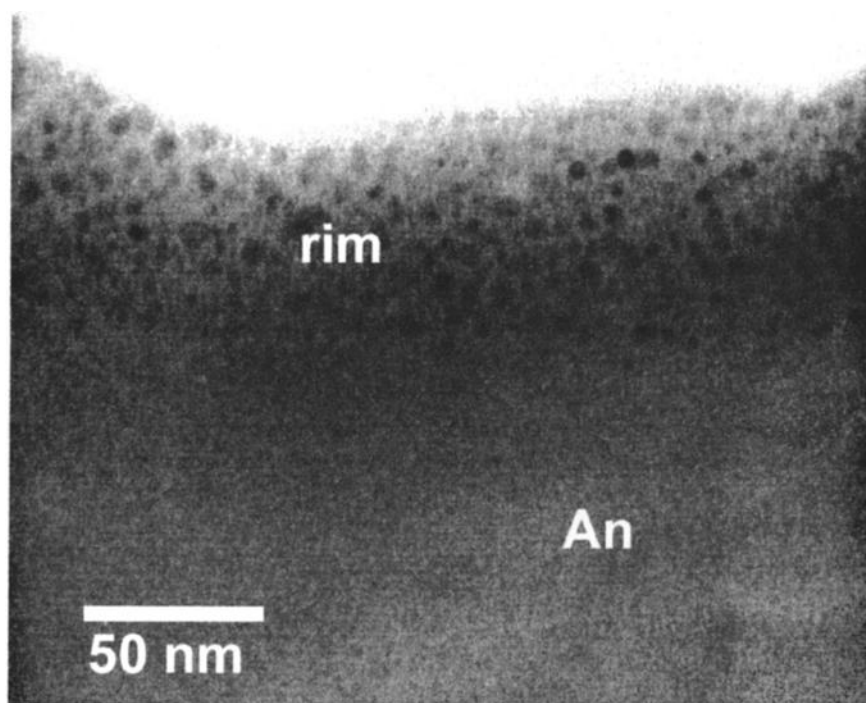
Figure 20. Transmission electron microscope image of a portion of an anorthite grain from lunar soil 79221 with a SMFe-rich coating. The dark spots in the rim are metallic Fe spherules. Photo courtesy of L. Keller.

partially reduced by prolonged baking in hydrogen show how difficult this is to achieve without special conditions.

4. The ferrous ions are reduced by impact melting of mineral grains saturated with solar wind hydrogen [*Housley et al.* 1973]. This hypothesis is widely accepted as the explanation for the SMFe and is virtually a paradigm in the lunar science community. The proposed process is a two-step one, in which the surfaces of the soil grains are first saturated with embedded solar wind hydrogen and then the grains are melted by a meteorite impact. During the high temperature vitrification the embedded hydrogen is hypothesized to reduce ferrous iron by the reaction $FeO+2H \longrightarrow Fe+H_2O$ and also to produce microscopic vesicles. This model is attractive because it simultaneously explains the SMFe and the vesicles found in the agglutinates.

However, there are several severe difficulties with the model: (1) This process may, in principle, be able to account for the SMFe in the agglutinitic glass, but it is incapable of explaining the SMFe found in the vapor-deposited rims on unmelted mineral fragments in lunar soil, particularly on the Fe-free plagioclase. (2) The reduction of Fe^{2+} is not necessary to explain the vesicles; the localized high transient pressure of embedded H is sufficient. (3) The SMFe particles should be intimately associated with the vesicles; however, this does not appear to be the case in either the agglutinitic glass or the coatings. (4) Some of the H_2O should have remained in the glass during solidification. However, there is no indication of native water in the soil; all of the trace water found in the Apollo samples appears to be terrestrial contamination [*Epstein and Taylor*, 1974]. (5) The process has no laboratory support.

E. Wells and the author attempted to test the *Housley et al.* [1973] mechanism as follows. A thin section of artificial silicate glass with FeO ~ 15% (approximating the composition of Apollo 11 rocks) was prepared and cut into three samples of equal size. Their transmission spectra were measured. They were then irradiated side - by - side by 2 keV H ions to a total dose of 30 C. The transmission spectra of one sample was again meausred. The other two samples were immediately placed one on top of the other with their irradiated surfaces in contact in a graphite strip furnace in vacuo. They were rapidly heated to 1230° C, where incipient melting was observed, and then cooled in vacuo. The heating and cooling took about a minute, and simulated the impact heating of a ferrosilicate whose surface contained imbedded H. The samples were then separated and one of them was measured. The absorbance spectra of the thin sections before irradiation, after irradiation, and after the vacuum - heating are shown in Figure 21. The spectra are identical within measurement error, showing that SMFe sufficient to affect the spectrum was not produced in this experiment either by H ion irradiation of the solid surface [section 4.3.2] or by near-melting *of a surface containing embedded H.*

4. The iron is reduced during deposition of vapors generated by solar wind sputtering and impact vaporization [*Hapke et al.*, 1975a]. This mechanism is consistent with all the observational evidence reviewed in sections 3 - 5. It accounts for the optical effects, the SMFe, the FMR, the enrichment of Fe metal on the grain surfaces, and the SMFe-bearing coatings. It has strong experimental support. The SMFe occurs natually as a by - product of the deposition process and requires no special conditions. The objection

frequently leveled at this hypothesis in the past, that there is no evidence for vapor deposits in the soil, has now been thoroughly refuted by the impressive TEM measurements by Keller and his colleagues described in section 5.8.

7. Vapor Deposition Model of Space Weathering

7.1. Model

The vapor - deposition model of lunar space weathering was introduced by the author and his colleages in three papers [*Hapke*, 1973; *Hapke et al.*, 1975a; *Cassidy and Hapke*, 1975]. These were based partly on earler sputtering studies by Wehner and his colleagues [*Rosenberg and Wehner*, 1964; *KenKnight et al.*, 1967] and by the author [*Hapke*, 1965; 1966; 1968]. The model was elaborated in several successive papers [*Wells and Hapke*, 1977; *Hapke and Cassidy*, 1978; *Paruso et al.*, 1978], and extended to Mercury by *Hapke* [1977] and *Rava and Hapke* [1987], to the asteroid belt in *Hapke* [2000], and to the outer solar system in *Hapke* [1986]. Previous attempts at quantitative spectral modeling were reported in *Hapke et al.* [1975a] and *Hapke* [1993b, 2000], and also by Shkuratov and his colleagues [*Starukhina et al.*, 1994; *Shkuratov and Starukhina*, 1999].

The space weathering model starts from the lunar regolith maturation model of McKay and his colleagues [*McKay et al.*, 1974, 1989], in which the soil is considered to be the product of meteorite impact comminution, which tends to break the rocks and minerals up into smaller particles, and shock vitrification and agglutination, which welds some of the smaller fragments of minerals and glass into larger particles. If comminution and vitrification were the only processes operating, the soil would have a high albedo and strong absorption bands, because neither the rock nor glass fragments

are dark. However, the soil is also bombarded by kilovolt solar wind hydrogen ions, which erode the grains by sputtering, and by hypervelocity micrometeorites, which vaporize some of the material in addition to comminuting and melting. It will be shown below in section 7.3.1 that most of this sputtered and vaporized material is injected downward into the soil and coats the grains in its path, rather than escaping upward.

The process of condensation of the Fe-bearing silicate vapors is intrinsically reducing, as shown in section 6, and results in the production of SMFe-bearing coatings on the soil particles. The only role of hydrogen is as a sputtering agent, and it is not necessary for reduction. The sizes of the Fe particles in fresh coatings are so small that they produce only a weak FMR. However, annealing by rapid heating and cooling can cause the Fe particles to grow into the size range where they have a strong FMR. This annealing can be done by heating by the same impact that produced the vapor or by a later one. Shock comminution and dispersal of native Fe in the lunar rocks and in impacting meteorites also contribute to the SMFe in the soil [*Morris*, 1980].

Succeeding impacts may dislodge some of the coatings which because of their small sizes cling to nearby larger particles. Impact vitrification also incorporates some of the coated grains into agglutinitic glass in which the SMFe is dispersed throughout the glass [*Hapke et al.*, 1975a; *Kerridge*, 1996]. The model will be further elaborated in the succeeding sections of this paper.

7.2. Optical Properties of SMFe

It is clear that the phenomenon of space weathering is closely connected to the SMFe in the lunar regolith. In this section the optical properties of submicroscopic metallic particles will be reviewed to aid in understanding the role of
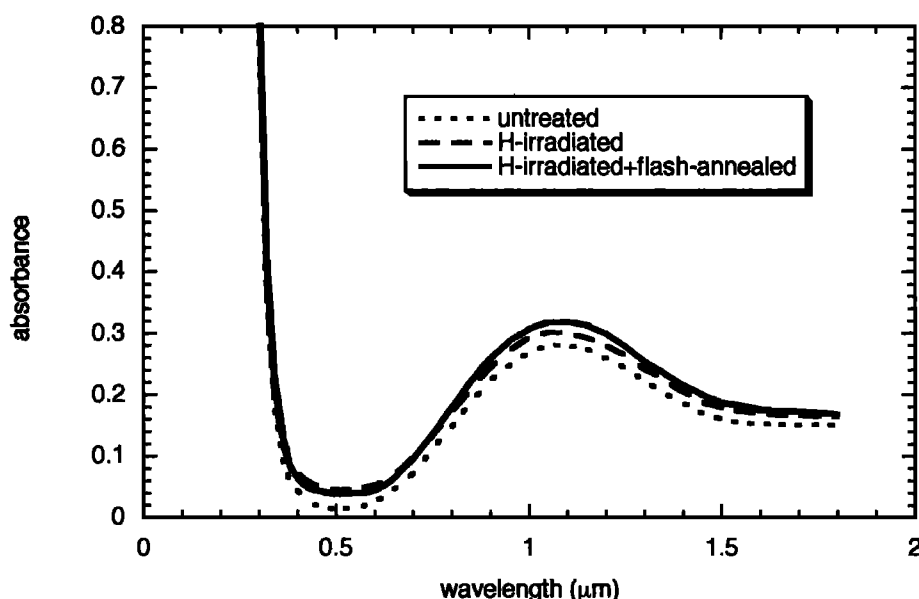

Figure 21. Absorbance spectra of a thin section of artificial glass, whose major element composition was the same as an Apollo 11 rock, before and after ion irradiation and flash annealing. See text for details.
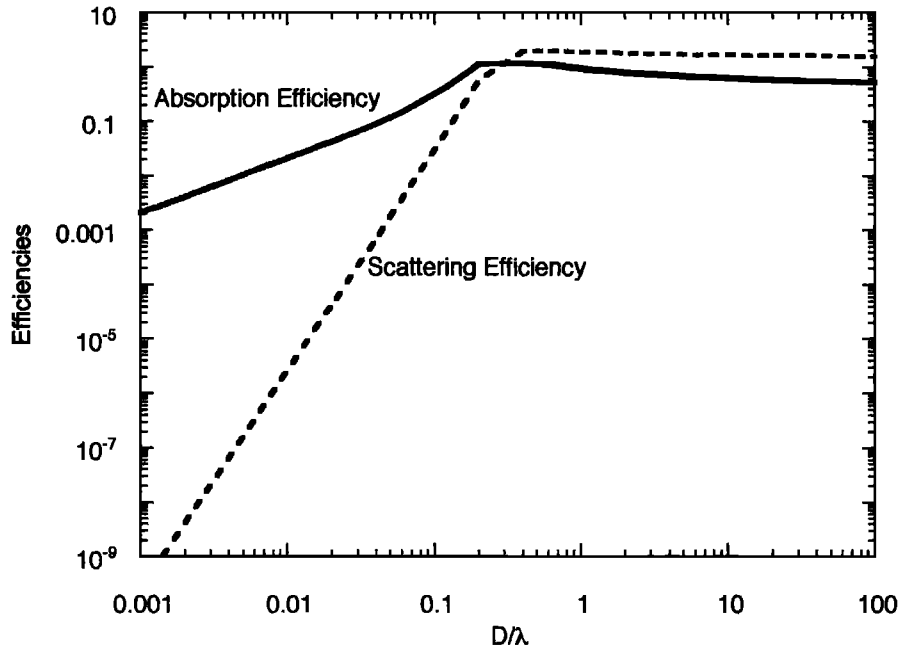
Figure 22. Absorption and scattering efficiencies plotted agains the ratio of diameter to wavelength of a sphere with refractive index (relative to its surroundings) $m = 3.0 + 3.0i$, calculated from Mie theory.

the SMFe. To illustrate the optical properties of metallic particles, consider a clear, nonabsorbing, nonscattering, transparent material containing metallic particles. These particles scatter and absorb light propagating through this medium. The absorption and scattering coefficients, α and s respectively, of the medium may be estimated in several ways. The expressions from radiative transport theory are

$$\alpha = \int N(D)\sigma(D)Q_A(D)dD , \tag{5}$$

$$s = \int N(D)\sigma(D)Q_S(D)dD , \tag{6}$$

where $N(D)dD$ is the number of metal particles per unit volume with sizes between D and $D+dD$, $\sigma(D)$ is the mean cross-sectional area of a particle of size D (for spheres $\sigma = \pi D^2/4$), $Q_A(D)$ is the absorption efficiency and $Q_S(D)$ is the scattering efficiency. The single scattering albedo of an individual particle is

$$w = Q_S/(Q_S+Q_A) . \tag{7}$$

Figure 22 shows the wavelength dependence of Q_A and Q_S of idealized spherical particles of refractive index relative to the host medium $m_m = 3.0+3.0i$ (which are typical values for metals in visible light) in a transparent medium. For illustrative purposes m_m is assumed to be independent of wavelength λ in Figure 22.

When $D > \lambda$, the efficiencies are almost constant, independent of size, and large, so that the particles absorb and scatter strongly, and their optical properties are virtually independent of λ. However, when the size decreases below about λ/π, the efficiencies decrease with decreasing λ. In this

region the efficiencies are given by the equations for Rayleigh scattering [cf. *Hapke*, 1993a],

$$Q_A = 4\frac{\pi D}{\lambda}Im(\frac{m_m^2-1}{m_m^2+1}) , \tag{8}$$

$$Q_S = \frac{8}{3}(\frac{\pi D}{\lambda})^4|\frac{m_m^2-1}{m_m^2+2}|^2 . \tag{9}$$

With decreasing λ, Q_A decreases as D/λ, while Q_S decreases as $(D/\lambda)^4$; hence, when $D << \lambda$ the particles are almost perfect absorbers. The absorption coefficient decreases as the wavelength increases so that light passing through the medium is reddened.

This simplified illustration assumed that m_m was independent of λ. However, the refractive index of most metals is not constant, but to a first approximation is described by the Drude model [cf. *Hapke*, 1993a], which predicts that m_m increases with λ. This behavior imposes a further wavelength dependence on the optical properties, such that both α and s tend to increase even more with wavelength than would be predicted if m_m were constant.

This dependence of the optical properties of metallic particles on size explains the spectral differences between the darkened and undarkened, gas-rich, ordinary chondrites studied by *Britt and Pieters* [1994], as due to the differing particle sizes of the Fe⁰ in these meteorites.

In the small particle region equation 8 shows that Q_A is proportional to D, so that α is proportional to $\int N(D)D^3dD$; however, the bulk density of the metal particles is $\rho_b = \int N(D)\rho_{Fe}(\pi D^3/6)dD$, where ρ_{Fe} is the solid density of the metal
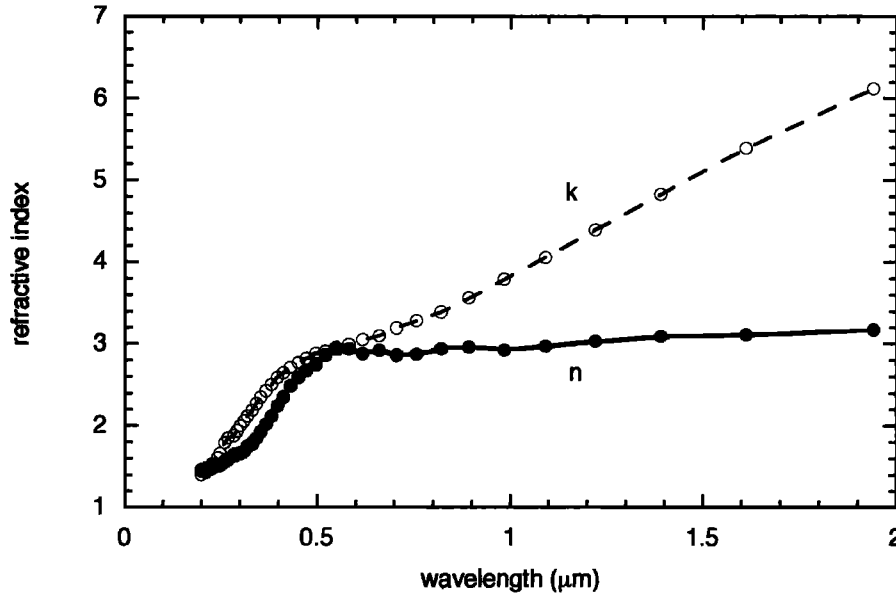
Figure 23. Real (n) and imaginary (k) parts of the refractive index of Fe^0 as measured by *Johnson and Christy* [1974].

particles. Hence α is independent of the particle size distribution and is proportional only to the bulk metal density. It should also be noted that particles smaller than λ are much more efficient absorbers per unit mass than particles larger than λ, because the entire small particle interacts with the light, whereas in a large particle the interior is shielded from the electromagnetic fields.

An alternate method of calculating the absorption coefficient is to use an effective medium model. In principle, this is more accurate than equations (5) - (8), because coherent effects between particles are taken into account. Maxwell-Garnett theory has considerable experimental support; hence the Maxwell-Garnett effective medium theory [cf. *Bohren and Huffman*, 1983; *Hapke*, 1993a] will now be used to calculate the absorption coefficient of a silicate host medium containing inclusions of small Fe metal spheres.

In the Maxwell-Garnett model the dielectric constant of a medium with inclusions is given by

$$K = K_h \left(1 + \frac{3\phi \dfrac{K_{Fe}-K_h}{K_{Fe}+2K_h}}{1-\phi \dfrac{K_{Fe}-K_h}{K_{Fe}+2K_h}} \right), \qquad (10)$$

where $K = m^2 = K_r+iK_i = n^2-k^2+2ink$ = dielectric constant of the medium containing the inclusions, $K_h = m_h^2 = K_{hr}+iK_{hi}$ = dielectric constant of the host material, $K_{Fe} = m_{Fe}^2$ = dielectric constant of Fe, ϕ = volume fraction of Fe particles, $m = n+ik$ = refractive index of the inclusion-bearing medium, $m_h = n_h+ik_h$ = refractive index of host material, $m_{Fe} = n_{Fe}+ik_{Fe}$ = refractive index of iron.

We will only be interested in the case where $\phi \ll 1$; hence, equation (10) may be expanded in a Taylor series in ϕ and only

terms to first order retained. Since k is proportional to ϕ, $k \ll n$; hence, $n \approx K_r^{1/2}$ and $k \approx K_i/2n$. From the dispersion relation [cf. *Hapke*, 1993a], $\alpha = 4\pi k/\lambda$. Using these approximations and relations, a straightforward calculation shows that the absorption coefficient of the medium is $\alpha = \alpha_h + \alpha_{Fe}$, where α_h is the absorption coefficient of the host material and α_{Fe} is the contribution of the Fe inclusions,

$$\alpha_{Fe} = \frac{36\pi}{\lambda}\phi z, \qquad (11)$$

where

$$z = \frac{n_h^3 n_{Fe}k_{Fe}}{(n_{Fe}^2-k_{Fe}^2+2n_h^2)^2+(2n_{Fe}k_{Fe})^2}. \qquad (12)$$

The spectral refractive index of Fe measured by *Johnson and Christy* [1974], shown in Figure 23, was used to calculate $\alpha_{Fe}[\lambda]$ for SMFe particles with $\phi = 0.0021$ imbedded in a silicate medium with $m_h = 1.70+0i$. The spectrum of α_{Fe} is shown in Figure 24. Note that the absorption coefficient decreases monotonically with increasing wavelength. The calculated quantity α_{Fe} normalized at 550 nm is also plotted in Figure 10, where it is seen to be similar to the measured absorbances of the SMFe-bearing films made by sputter and vapor deposition of lunar materials.

Finally, it must be emphasized that the optical effects of space weathering are caused by all of the Fe particles that are smaller than the wavelength, and not just by the nanometer-sized particles involved in the FMR. For this reason this paper uses SMFe, rather than npFe⁰, to refer to the space weathering carrier.
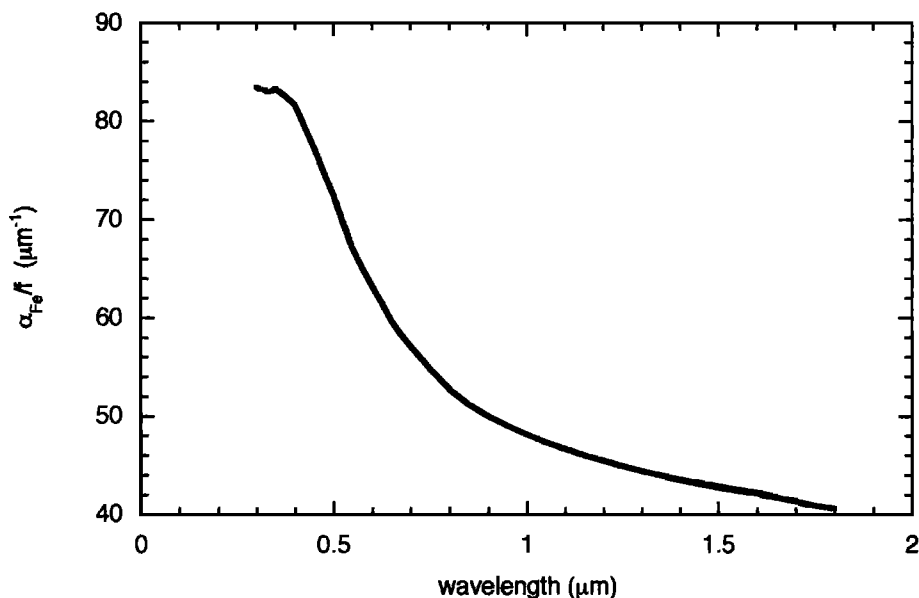
Figure 24. Spectrum of absorption coefficient α_{Fe} divided by mass fraction f of Fe^0 of a material with $m =$ $1.70+0i$ containing SMFe, calculated from the Fe data of *Johnson and Christy* [1974] using effective medium theory.

7.3. Vapor Deposits in the Lunar Regolith

7.3.1. Retention in the soil. A frequent objection to the vapor deposition hypothesis is that the vapors generated by impacts and sputtering will have large upward velocities and, thus, be lost from the Moon. However, this argument applies only to a flat, smooth, planetary surface, and is completely wrong for a porous, particulate, highly reentrant medium like the lunar regolith. Consider first the sputtering process. In section 4.3.5 it was pointed out that many of the incident ions pass between the particles in the top soil layer and sputter material from the particles in lower layers. Most of this sputtered material coats the undersides of particles in the upper layers. More importantly, however, atoms sputtered by the ions that are incident at glancing angles onto the sloping sides of the soil particles tend to preserve the momentum of the incident ions and are sputtered preferentially downward into the powder, where they coat the underlying particles.

The ability of a porous powder to retain sputtered material is illustrated in an experiment reported by *Hapke and Cassidy* [1978]. Two sputter targets were prepared . One was a solid glass bead 7 mm in diameter of basaltic composition. The second target consisted of the same glass ground to finer than 37 μm and lightly sintered into the form of a glass bead 7 mm across. Both were irradiated side - by - side by a beam of 2 keV H ions at a current density of 0.3 mA cm⁻² for 60 hours. Midway through the irradiation, the positions of the samples were reversed. The samples were weighed before and after the irradiation. The solid bead lost 2.1 mg cm⁻², while the porous bead only lost 0.20 mg cm⁻². Thus over 90% of the atoms sputtered by the solar wind were retained in the powder. Moreover, *Carey and McDonnell* [1976] carried out a Monte Carlo calculation in which they modeled atoms ejected isotropically into the upward hemisphere from a heavily

cratered, but microscopically smooth surface. They found that up to 70% of the ejected atoms would strike the sides and floors of the craters and be retained. The combination of the two effects shows that approximately 97% of the atoms sputtered on the Moon by the solar wind remain in the regolith.

Next, consider hypervelocity impacts. The size distribution of meteorites in space is concentrated in the smaller sizes, similar to the lunar regolith. Most of the objects hitting the surface of the Moon have diameters of tens to hundreds of micrometers [*Gault et al.*, 1972]. The surface they strike is not a flat, horizontal, solid half-space, but consists of particles roughly the same size as the impactor and arranged in a fluffy, porous, "fairy - castle" packing. The following crude calculation indicates the order of magnitude of the phenomena to be expected in such an event.

Consider a micrometeorite of mass M and velocity V_0 impacting a regolith particle of similar mass M. Following the initial contact, a shock wave proceeds forward into the target particle and backward into the impactor. At the instant the shock waves have reached the far ends of the particles, the two grains have merged into a single system of mass $2M$, which may be considered to be temporarily isolated because of the highly porous regolith. By conservation of momentum, the velocity of the combined system at this time is $V = MV_0/2M =$ $V_0/2$, and its kinetic energy is $KE = (1/2)(2M)(V_0/2)^2 =$ $MV_0^2/4$, which is half of the initial kinetic energy. The other half has been converted into internal energy. The increase in internal energy per unit mass of the combined system is $IE =$ $(MV_0^2/4)/(2M) = V_0^2/8$. This is plotted in Figure 25.

For an initial velocity of $V_0 = 15$ km s⁻¹, $IE \approx 3 \times 10^7$ J kg⁻¹. By comparison, the free energy of formation (the energy required to dissociate a compound into its constituent
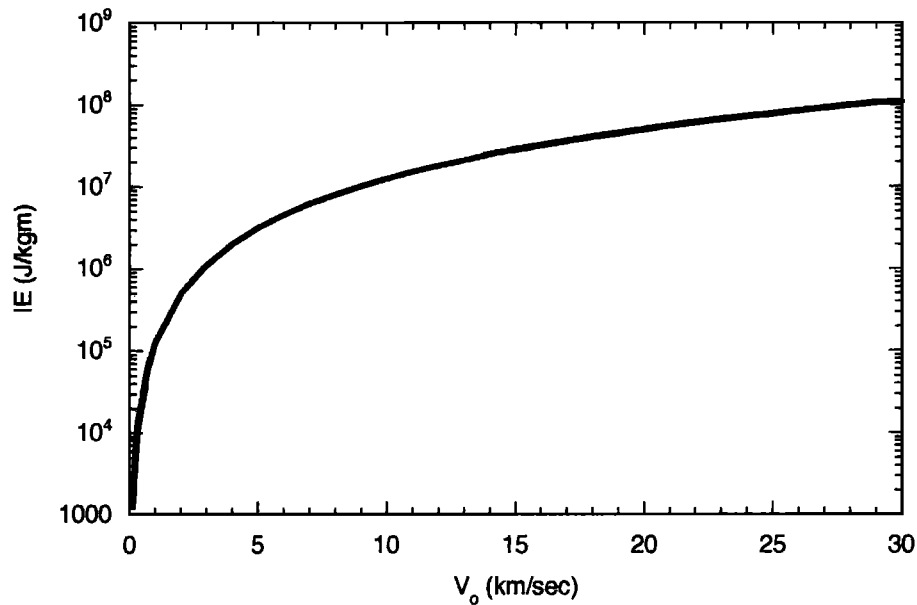
Figure 25. Increase of specific internal energy during the initial stages of an impact plotted against impact velocity.

elements) of forsterite is 1.5×10^7 J kg^{-1} [*Stull and Prophet*, 1971]. Hence at this stage the system consists of a high - density, high - temperature cloud of vapor whose center of mass is moving downward into the regolith at half the initial impact velocity. Because there is nothing to confine the cloud, it expands rapidly before contacting the other particles in the regolith, so that it is likely that a considerable fraction remains in vapor form and plates out onto the surrounding soil grains. *Starukhina et al.* [1999] estimated that the condensation products would be distributed over a layer whose thickness is several times the diameter of the impactor. As the cloud interacts with the regolith, the kinetic energy is converted into other forms, such as melting, comminution and excavation. Finally, a secondary source of condensates is evaporation from impact - melts.

In summary, theoretical arguments indicate that almost all of the vapor generated in a planetary regolith by both sputtering and meteoritic impacts should be retained in the regolith. These arguments have been experimentally verified in the case of sputtering. To the author's knowledge, no hypervelocity impact experiments or computer models have simulated an impact into a porous medium composed of particles of the same size as the impactor, even though this is probably the most common process on the lunar surface. However, these kinds of experiments and model calculations should be done to test these conclusions.

7.3.2. Amount of vapor deposits in the lunar regolith.. A number of persons have attempted to estimate the rates of vitrification, vaporization, and sputtering on the lunar surface. These estimates are summarized in Table 2. Although these values are highly uncertain, it can be seen that the amount of vapor generated by sputtering plus impacts is comparable to the amount of material melted. The amount of glass in a mature regolith exeeds 50% [*Taylor et al.*, 1999a], of which Table 2 suggests that of the order of one half may be vapor deposits.

From their magnetic measurements, *Hapke et al.* [1975a] estimated that SMFe makes up roughly 10% of their experimentally - produced, evaporated films. Since the lunar regolith contains ~ 0.5% SMFe, this implies that vapor deposits constitute ~5% of the soil. Another estimate can be made from the specific surface area SSA (section 2.6). If it is assumed that all exposed surfaces are covered with vapor - deposited coatings of thickness $t \sim 100$ nm and density $\rho = 3$ g -cm^{-3}, they would consititue a fraction ~ SSA$t\rho$ = 15% of the regolith.

Thus it is clear that vapor deposits are a major component, making up 5 - 25% of the lunar regolith. If the optical, magnetic, chemical, and isotopic properties of the regolith are to be understood, vapor phase transport and deposition cannot be neglected [*Hapke et al.*, 1994].

8. Model and Applications of the Optical Effects of Space Weathering

8.1. General Proceedure

To model the optical effects of the SMFe produced in the space weathering process, the equations developed in *Hapke*

Table 2. Rates of Generation of Melt Glass and Vapor Products on the Lunar Surface, g cm^{-2} yr^{-1}

Reference	Impact Melt	Imapct Vapor	Sputter Products
Wehner et al [1963]			3
Gault et al. [1972]	6	2.6	
Maurette and Price [1975]			15
McDonnell [1977]			1
Morgan et al. [1989]		25	
Johnson and Baragiola [1991]			1 - 2
Cintalla [1992]	14	2 2	
Averages	10	10	5

[1993a] based on radiative transfer theory will be used. In order to simplify the calculations, several assumptions will be made. The particles are assumed to be isotropic scatterers, and the opposition effect is ignored, since it is not crucial and can be readily included in more sophisticated models. The theory requires the specification of several parameters, the values of which may be estimated from prior knowledge of the medium or found by fitting to observational data. These parameters are n, α, s and D, which are, respectively, the real part of the refractive index, absorption coefficient, internal scattering coefficient, and effective particle size of the particles in the media. In the following, a subscript h on these symbols indicates the unweathered host medium, and subscript w indicates the weathered SMFe-bearing soil.

Appropriate expressions must be used depending on whether the observed reflectances are bidirectional or directional-hemispherical (hemispherical albedo), physical albedo, or some other type of reflectance or albedo. The bidirectional reflectance of a medium of isotropic scatterers of single - scattering albedo w is given by

$$r(i,e,g) = \frac{w}{4\pi} \frac{\mu_0}{\mu_0+\mu} H(\gamma,\mu_0)H(\gamma,\mu) , \qquad (13)$$

where i is the angle of the incident ray from the surface normal, e is the angle of the emergent ray from the normal, g is the phase angle, $\mu_0 = \cos i$, $\mu = \cos e$, w is the single scattering albedo, $\gamma = (1-w)^{1/2}$, and $H(\gamma,x) = (1+2x)/(1+2\gamma x)$ is an analytic approximation to the Ambartsumian - Chandrasekhar H - functions. Most reflectances are relative to a standard, which may be taken with little error to be a particulate medium whose single scattering albedo is 1.00 measured at the same angles. Then the relative reflectance is

$$\Gamma(\gamma) = \frac{r(\text{sample})}{r(\text{standard})} = \frac{1-\gamma^2}{(1+2\gamma\mu_0)(1+2\gamma\mu)}, \qquad (14)$$

which may be solved for γ,

$$\gamma = \frac{[(\mu_0+\mu)^2\Gamma^2+(1+4\mu_0\mu\Gamma)(1-\Gamma)]^{1/2}-(\mu_0+\mu)\Gamma}{1+4\mu_0\mu}, \qquad (15)$$

from which the single scattering albedo of the sample may be found from $w = 1-\gamma^2$.

If the reflectances are hemispherical, the appropriate expression to use instead of equation (13) is the hemispherical reflectance relative to a perfect diffuse reference,

$$r_H(i) = 1 -\gamma H(\gamma,\mu_0) = \frac{1-\gamma}{1+2\gamma\mu_0}, \qquad (16)$$

which may be solved for γ,

$$\gamma = \frac{1-r_H}{1+2\mu_0 r_H}. \qquad (17)$$

The single - scattering albedo is related to the properties of an average particle of the medium by

$$w = S_e+(1-S_e)\frac{1-S_i}{1-S_i\Theta}\Theta , \qquad (18)$$

where S_e is the Fresnel reflection coefficient of the surface of the particle averaged over all angles of incidence for light incident on the particle surface from outside the particle and S_i is the average Fresnel reflection coefficient for light incident from inside the particle. For nonmetallic particles with imaginary refractive index $<< 1$ the following are good approximations:

$$S_e = (n-1)^2/(n+1)^2 + 0.05, \qquad (19)$$

$$S_i = 1-4/n(n+1)^2. \qquad (20)$$

The parameter Θ is

$$\Theta = \frac{r_i+\exp(-\sqrt{\alpha(\alpha+s)}\,D)}{1+r_i\exp(-\sqrt{\alpha(\alpha+s)}\,D)}, \qquad (21)$$

$$r_i = \frac{\sqrt{1+\alpha/s}-1}{\sqrt{1+\alpha/s}+1}, \qquad (22)$$

where s is the internal scattering coefficient, α is the absorption coefficient, and D is the mean photon path length through the particle. Note that if the particle has no internal scatterers, $s = 0$ and Θ is the single-pass transmission of the particle, $\Theta = \exp[-\alpha D]$; if $\alpha D >> 1$, $\Theta = r_i$.

Solving equation (18) for Θ gives

$$\Theta = [S_i+\frac{(1-S_e)(1-S_i)}{w-S_e}]^{-1}. \qquad (23a)$$

If $s = 0$, $\Theta = \exp[-\alpha D]$, from which α may be found:

$$\alpha = \frac{1}{D}\ln[S_i+\frac{(1-S_e)(1-S_i)}{w-S_e}]. \qquad (23b)$$

In these equations the surface scattering parameters S_e and S_i can be calculated using equations (19) and (20).

The procedure for modeling a regolith is as follows. Starting with the measured spectral reflectance of unweathered material, the reflectance equations are inverted to give the host absorption coefficient α_h using equations (13) - (23). Next, the absorption coefficient of the SMFe is added to that of the host grain to find $\alpha_w = \alpha_h+\alpha_{Fe}$, where α_{Fe} is calculated from the measured complex refractive index of Fe using equations (11) and (12). Finally, the single scattering albedo and reflectance of the weathered regolith are calculated using equations (13) - (23).

The first step is to invert the appropriate expression for the reflectance of the unweathered host material (equation (15) or (17)) to find γ_h and w_h. It is assumed that $s = 0$, and α_h is found using equations (18) - (23). Next, α_w is calculated using

equations (11) and (12) for α_{Fe}, in which the values of the complex refractive index of Fe are taken from *Johnson and Christy* [1974], and added to α_h to give α_w. Here we encounter a problem: The measured values for Fe in the literature are inconsistent with each other, differing by as much as a factor of 2. The reason is uncertain, but is probably connected with the degree of oxidation of the surfaces of the Fe samples used in the various measurements. The Johnson and Christy values have been arbitrarily chosen because they are the only ones that cover the entire wavelength range of interest here.

The SMFe inclusions in the soil can either be uniformly distributed throughout a particle or concentrated in coatings. If the SMFe inclusions are uniformly distributed within the entire particle then the volume fraction of iron is $\phi = \rho_{Fe}f/\rho_h$, where ρ_h is the density of the host material, ρ_{Fe} is the solid density of Fe and f is the bulk mass fraction of the Fe particles, so that

$$\alpha_w = \alpha_h + 36\pi z f \rho_h/\lambda\rho_{Fe}. \qquad (24a)$$

This expression applies whether or not there are internal scatterers.

Next, consider the case where the inclusions are in rims. First, suppose $s = 0$, and consider a bundle of rays traversing a typical path of length D and cross-sectional area da through a particle. Let the particle be uniformly coated with a rim of thickness $t \ll D$. Then the volume of coating along the path is $2tda$, the volume of iron in the rim along the path is is $2\phi tda$, where ϕ is the volume fraction of Fe in the rim, and the volume of the host material along the path is Dda. Thus the mass fraction of iron in the entire particle is $f = 2\rho_{Fe}\phi tda/\rho_h Dda$, so $\phi = \rho_h Df/2\rho_{Fe}t$, and the absorbance along the path is

$$\alpha_h D + \alpha_{Fe}2t = \alpha_h D + [36\pi z f \rho_h/\lambda\rho_{Fe}]D = \alpha_w D. \qquad (24b)$$

Hence the effect of the rim is to multiply the quantity Θ in the expression for w by $\exp[-(36\pi z f \rho_h/\lambda\rho_{Fe})D]$. The same is true when $s \neq 0$: The value of Θ calculated for the case of $s > 0$ (equations (21) and (22)) is multiplied by $\exp[[-36\pi z f \rho_h /\lambda\rho_{Fe}]D]$ and the result inserted into the expression for w.

To illustrate this proceedure and the spectral effects of the SMFe, a simple example will be given. Consider an idealized regolith consisting of particles 10 μm in size of a mineral with $n_h = 1.70$. Assume that the hemispherical reflectivity of the host medium normally illuminated is $r_{Hh} = 32\%$ and flat except for a Gaussian absorption band at $\lambda = 1$ μm. Applying equations (19), (20) and (23) gives $S_e = 0.12$, $S_i = 0.68$, and the continuum absorption coefficient is 0.00637 μm^{-1}. To this, add a Gaussian such that the host absorption coefficient is $\alpha_h = 0.00637+0.003\exp[-(\lambda-1)^2/0.05]$ μm^{-1}. The resulting reflectance spectrum is shown as the curve labeled "f = 0" in Figure 26. Assume that the SMFe is in coatings of the same n_h on the grains and that $s_h = 0$. Then $\alpha_w D = \alpha_h D + [36\pi z f \rho_h /\lambda\rho_{Fe}]D$, where z is given by equation (12) using the Fe data of *Johnson and Christy* [1974]. These quantities are then inserted into equations (16) and (18) to give the hemispherical spectral reflectance r_{Hw} of the weathered material. These spectra are illustrated in Figure 26 for $f = 0$, 0.1%, 0.5%, and 2%.

The changes in spectral shape as the amount of Fe^0 increases may be understood as follows. The overall spectrum of the iron-free sample is flat (except in the band) and the reflectance is determined by its intrinsic absorption coefficient.
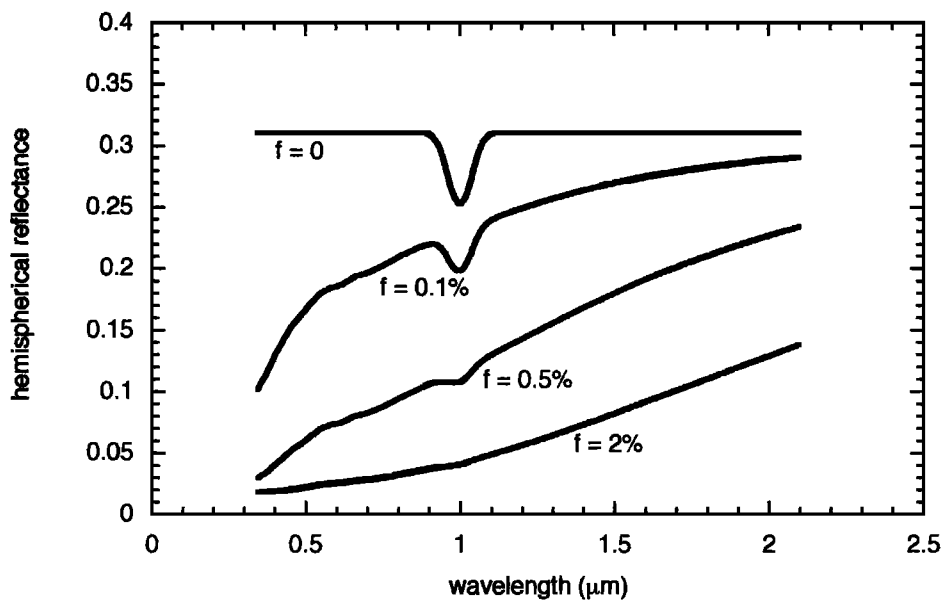

Figure 26. Theoretical hemispherical reflectance spectra of a particulate medium of 10 μm particles, showing effect of adding SMFe on the amplitude and shape of the spectrum and the depth of an absorption band. See text for details.

Adding 0.1% SMFe decreases the blue end of the spectrum more than the red end because of the stronger absorption at short wavelengths. The shape of the continuum spectrum is convex - upward in the blue and relatively flat in the red. The SMFe depresses the continuum reflectance relatively more than the band center, so that the relative band depth decreases. This convex - upward behavior is also seen in the spectra of the lunar soil size separates in Figure 3. It is especially marked for the < 10 μm fraction and is also seen in the spectra of many S - asteroids.

Increasing the Fe content to 0.5% reduces the short - wavelength reflectance until the sample becomes so absorbing in the UV that only light reflected from the grain surfaces contributes to the reflectance. However, the long wavelengths are not strongly absorbed, and the reflectance remains high in the red. Light of intermediate wavelengths is partially absorbed, so that the continuum spectrum approximates a straight line.

In the spectrum with a SMFe content of 2%, the absorption by the SMFe is so large in the blue region of the spectrum that the reflectance has bottomed out at the value determined by the Fresnel reflection S_e from the grain surfaces. Because S_e is assumed to be independent of wavelength, the reflectance is small and flat. Some light that has been refracted through the interiors of the grains still contributes to the long wavelength reflectance, and the shape of the spectrum is concave - upward there. The absorption band has been completely obscured.

Allen et al. [1996a] prepared silica gels containing inclusions of Fe_2O_3 6 nm in diameter and reduced the oxide to metallic Fe by heating in a hydrogen atmosphere. The reflectance spectra of their experimental gel powders are qualitatively similar to Figure 26.

8.2. Lunar Regolith

Applying this model to the Moon, the host spectra were taken to be the measured bidirectional reflectances [relative to a $BaSO_4$ standard] of an Apollo 11 lunar rock, sample 10017, and a glass made by vitrifying this rock in vacuum, both ground to < 37 μm. Both sample and standard were measured at $i = e = 30°$ and $g = 60°$. The spectra of these samples are shown in Figure 27. The lunar rocks are mafic materials, for which refractive indices of 1.7 are typical.; hence, $n_h = 1.70$ was used for both the rock and glass at all wavelengths. Applying equations (15) and (23) to these spectra gives w_h of the rock and glass powders. In the work by *Hapke and Wells* [1981](see also Hapke [1993a]), the reflectance spectra of artificial glass powders < 37 μm in size with known absorption coefficients were fitted by equations of the form of (17) and (18). A good fit was obtained with the internal scattering coefficient equal to zero and the equivalent optical path length equal to 16 μm. Hence, we take $s_h = 0$ and $D_h = 16$ μm for both the lunar rock and glass powders.

It is assumed that the SMFe is all in coatings on the grains of rock powder, but is distributed throughout the volumes of the glass particles in the agglutinates. The weathering effects

are added by calculating α_w and w_w using equations (18) and (24). The mass fraction of Fe is taken to be 0.5%, which is typical for lunar samples. The equivalent optical path length through the lunar particles is chosen to be the mean grain size weighted by cross - sectional area $D = D_p = 26$ μm, consistent with the discussion in section 2.5. The large SSA of the soil (section 2.6) is interpreted as implying that the soil particles are filled with highly reentrant cavities which act as internal scatterers. Hence it is unlikely that $s_w = 0$, so s_w is taken as a parameter to be fitted. The soil is assumed to be an intimate mixture of 50% rocks and 50% glass, and the single - scattering albedos of the two components are calculated and averaged to give the w_w of the soil. Finally, the relative bidirectional reflectance spectrum $\Gamma_w(\lambda)$ of the model soil is calculated from equation (14). The result is compared with the measured spectrum of soil sample 10084.

This procedure was repeated for several values of s_w. The best match was found to be for $s_w = 6$. The internal scattering parameter s_w can be loosely interpreted as the number of scattering surfaces encountered by a photon as it traverses a typical particle. The SSA, which is equivalent to a medium of particles 4 μm in size, can be interpreted as caused by a large number of reentrant surfaces in a soil particle. Hence it is expected that $s_w \sim D_p/4 = 6.5$, in good agreement with the best fit value of $s_w = 6$.

The calculated and measured spectra of the soil are shown in Figure 27. The fit is seen to be excellent except at the longest wavelengths. The reason for the poorer fit there is unclear, but may be the uncertainty in the measured refractive index of Fe, or it may be caused by Fe particles larger than the wavelength, which are not accounted for in the model.

A final interesting question is whether sputter - deposition or impact vapor - deposition dominates the space weathering of the lunar regolith. This cannot be answered at present, but it is likely that both processes are important. Further detailed analyses of the compositions of the particle coatings may illuminate this question.

8.3. Mercury

The first high - quality, broad - band spectrum of Mercury was obtained by *McCord and Adams* [1972]. It seemed to be similar to the spectrum of the Moon, including an apparent pyroxene band near 1 μm. This resemblance led these workers to suggest that the crust of Mercury was a high iron-titanium silicate like the lunar maria. However, water vapor in the Earth's atmosphere has a band near 1 μm, and it is extremely easy for this band to contaminate a spectrum, particularly when looking at an object near the horizon. *Hapke et al.* [1975b] were unable to reconcile the color and albedo relationships imaged by the Mariner 10 spacecraft with a high iron content and suggested that the surface was low in iron and titanium. This inference received strong support from telescopic spectral measurements by *Vilas* [1988] who was unable to reliably detect a 1 μm band. However, the low albedo and reddish
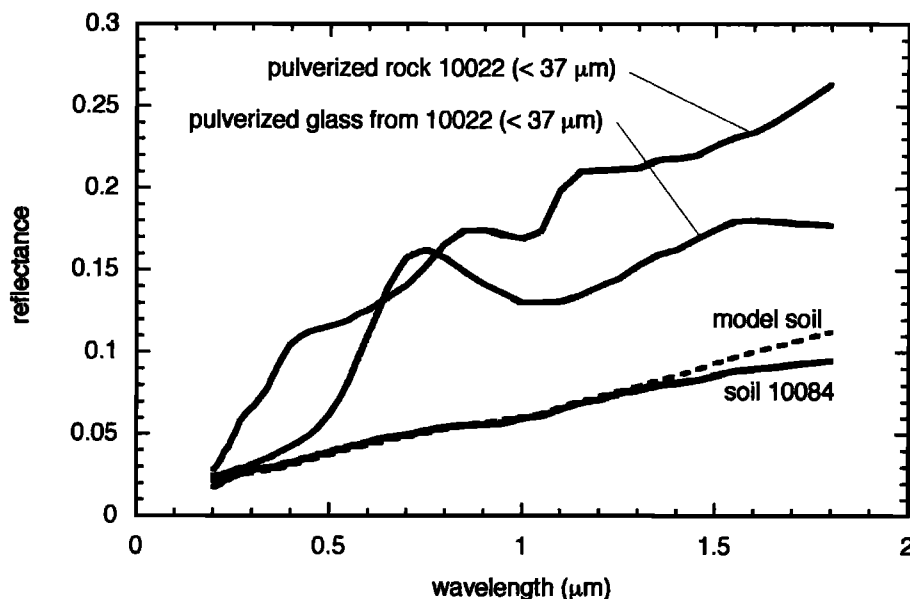
Figure 27. Modeling space weathering in lunar regolith. The figure shows the bidirectional reflectance spectra (i = 30°, e = 0, g = 30°, relative to a polytetrafluoroethylene [PFE] standard] of a pulverized lunar rock, a glass made from the rock and lunar soil from the same location. The dashed line is a theoretical regolith spectrum modeled by adding 0.5% SMFe to the rock and glass. See text for details.

slope of the spectrum is virtually identical to the Moon's, which strongly suggests a lunar type of space weathering caused by SMFe-bearing vapor deposits.

Space weathering effects on the regolith of Mercury have been discussed extensively by *Hapke* [1977] and *Rava and Hapke* [1987]. Mercury possesses a planetary magnetic field which, although weak, stands off the solar wind most of the time. However, solar wind ions can often reach the polar surface during substorms and reach the entire surface during periods of high solar activity. Hence a limited amount of space weathering by solar wind sputter deposition should occur. More importantly, the mean velocity of objects impacting Mercury is expected to be substantially higher than for the Moon. *Cintala* [1992] estimated that this factor causes 20 times as much vapor to be produced per unit time on Mercury as on the Moon. Thus impact vapor deposits should be even more abundant in Mercurian than in lunar regolith, and any ferrous iron present should have been partially converted to SMFe by vapor deposition.

The question of how much ferrous iron is present in the regolith cannot be definitively answered at present. From the nondetection of a 1 μm band, *Adams and McCord* [1977] estimated a highly conservative upper limit of 6% FeO, assuming that the crust is a mafic silicate darkened by lunar amounts of space weathering. From the spectrum and albedo, *Blewett et al.* [1997a] estimated that FeO+TiO$_2$ ≈ 4 %. Another possibility is that the Mercurian regolith formerly contained a large amount of FeO which has been nearly all converted to SMFe by efficient vapor deposition. This is unlikely because, as Figure 26 shows, a regolith that contains more than about 1% SMFe would have a low visual albedo and a spectrum that is concave - upward. Yet a third

possibility is that all of the native minerals are ferrous-free with only metallic Fe present, as in the enstatite chondrites. However, *Hapke* [1966] found that irradiating powdered chondrites and other materials with a high abundance of metallic Fe in a simulated solar wind caused them to have albedos that are too low and spectra that are too flat (see Indarch (E4) in table 1).

Thus present knowledge indicates that Mercury probably has a crust that is low in ferrous iron, but is not ferrous-free. The SMFe content of the regolith is probably similar to the Moon's, around 0.5 %. Better measurements of the shape of the short - wavelength spectrum of Mercury might allow this estimate to be improved.

8.4. Asteroid Regoliths: The Ordinary Chondrite, S Asteroid Connection

The S asteroids are the most common spectral class of asteroids in the inner belt, and the ordinary chondrites are the most common type of meteorite. For many years it has been a subject of considerable debate whether the first are the parent bodies of the second. This debate is the topic of several recent papers [*Bell et al.*, 1989; *Clark et al.*, 1992; *Chapman*, 1996; *Pieters et al.*, 2000] and will be only briefly summarized here. The ordinary chondrites and the S asteroids both have pyroxene and olivine absorption bands; however, as a class, the asteroid spectra have continuum spectra that are redder and bands that are more subdued than the chondrites. These differences are exactly the same as the differences between lunar rocks and soils from the same location, so that it is natural to speculate that a lunar type of space weathering also acts in the asteroid belt.

The space weathering mechanism postulated in this paper lowers the albedo. Whether or not the S asteroids as a class

are darker than the ordinary chondrites is unclear. The chondrite laboratory spectra are bidirectional or directional-hemispherical and are affected by such parameters as the size to which the meteorites are ground. By contrast, the asteroid spectra are integrated reflectances, such as physical albedo, taken at a variety of phase angles and are affected by several factors, including mean soil particle sizes (which are completely unknown), phase angle (especially the opposition effect), and rotational angle. For these reasons, usually only spectra arbitrarily normalized to each other are used for intercomparison.

A major difference between the environments of the Moon and asteroids is that meteorites with similar orbits as the asteroids strike asteroidal surfaces at much lower velocities. *Horz and Schaal* [1981] estimated that the mean impact velocities in the belt are around 5 km s^{-1}, which can cause comminution, but little melting or vaporization. *McKay et al.*[1989] concluded that asteroid soil should be immature compared with lunar soil. Because it was widely, but erroneously, believed that lunar space weathering is caused by impact vitrification, the possibility that a similar process acts on asteroidal surfaces has not been taken seriously.

However, now that the process is known to be caused by both impact vaporization and sputtering, it is appropriate to reconsider the problem. Even though the relative impact velocities are too low to allow appreciable vaporization, the solar wind still bombards the surfaces of the S - asteroids, and thus space weathering by sputter deposition must occur. Hydrogen ion irradiation has been demonstrated in the laboratory to darken and redden pulverized samples of a variety of types of meteorites [*Hapke*, 1968] (also Table 1). In this section it will be shown that the addition of sputter - deposited coatings containing SMFe on the surfaces of

regolith grains can make the spectrum of a pulverized ordinary chondrite strongly resemble that of an S - asteroid. The vapor - deposition model applied to asteroids is also discussed by *Pieters et al.* [2000].

The spectra of a powdered sample of an H6 ordinary chondrite, Nanjemoy, and an S - asteroid, 26 Proserpina, were chosen at random from *Clark et al.* [1992]. These spectra are shown in Figure 28. Because the photometric equations are nonlinear absolute, not relative, reflectance must be used to calculate the effects of space weathering. Hence the spectrum of Nanjemoy was renormalized to the value of the visual albedo given in their paper. This converted the spectrum of Nanjemoy to a bidirectional reflectance at $i = 30°$, $e = 0$ and $g = 30°$, relative to a diffuse standard. Assuming as in the previous section that the particles are isotropic scatterers, the reflectance is given by equation (14). This equation may be solved for the single scattering albedo w_h of the host meteorite grains using equation 15. The meteorite sample was ground to finer than 50 μm; from the results of *Hapke and Wells* [1981] the effective grain size is estimated to be $D_h = 25$ μm. And $s_h = 0$. Taking the real refractive index to be $n_h = 1.70$, w_h can be inserted into equation (23b) to find α_h.

Next the mean single scattering albedo of the asteroid regolith can be modeled using equations (21) and (24) after choosing values for the parameters in this equation. Take $n_h = 1.70$. If there are few agglutinates in the regoliths of asteroids, then the particles are not expected to have as many reentrant cavities as lunar soil particles; hence take $s_w = 0$. Since agglutinates are not expected, the SMFe should occur only in sputter-deposited rims on the particles; hence, Θ_w may be modeled simply as
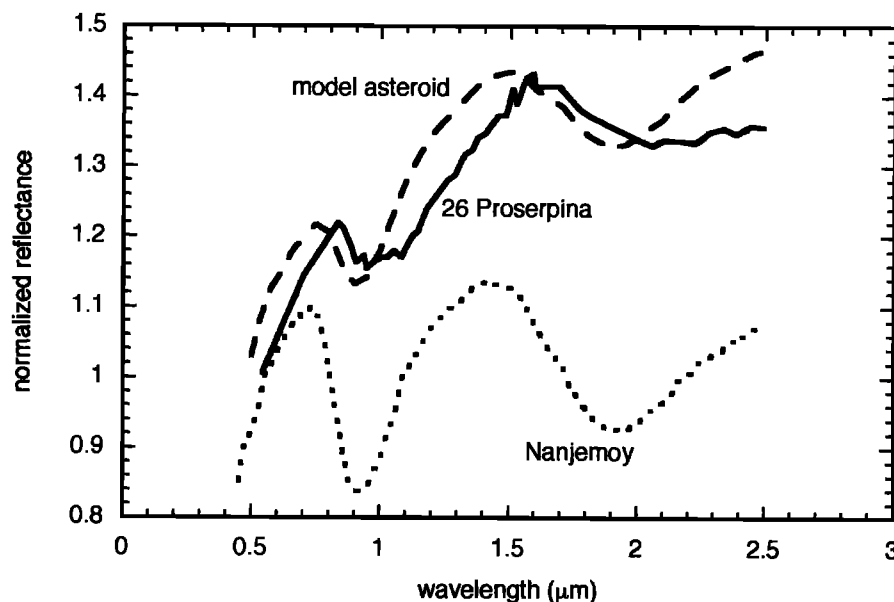

Figure 28. Modeling space weathering on an asteroid. The figure shows the bidirectional reflectance spectrum of Nanjemoy, an H6 ordinary chondrite, and the spectral physical albedo of 26 Proserpina, an S - asteroid. The dashed line is a theoretical regolith spectrum modeled by adding 0.025% SMFe to Nanjemoy. The spectra are arbitrarily nomalized. See text for details.

$$\Theta_w = \exp[-(\alpha_h + \alpha_{Fe})D],$$

where D is the mean photon path length through a typical asteroid regolith particle. Since we do not have any information on the particle size distribution in asteroid soils, D will be taken as a parameter to be fitted, along with f, the mass fraction of SMFe. The optical constants of Fe were measured by *Johnson and Christy* [1974] only for $\lambda < 1.8$ μm. They were extrapolated to 2.5 μm by fitting a second order polynomial to the data between 1.0 and 1.8 μm, and the result was used to calculate α_{Fe}.

The spectrum of the asteroid is assumed to be the spectral physical albedo. From *Hapke* [1993a] the physical albedo of a planet covered with a regolith of isotropic scatterers (ignoring the opposition effect) is given to a good approximation by

$$A_p = 0.49r_o + 0.196r_o^2, \tag{25}$$

where

$$r_o = \frac{1 - \sqrt{1 - w}}{1 + \sqrt{1 - w}}. \tag{26}$$

Trial values for D and f were used to calculate w_w, which was inserted into equations (25) and (26), and A_p was determined. As discussed previously, comparison of meteorite and asteroid absolute reflectances is impossible. Thus the model spectrum was arbitrarily normalized to the asteroid spectrum, and the two were compared. The procedure was then repeated for different values of D and f. The values of these parameters that gave the best fit were $D = 10$ μm and $f = 0.025\%$.

The best - fit spectrum is shown in Figure 28. As expected, addition of SMFe alters the meteorite spectrum so that it more closely resembles the asteroid: The meteorite spectral reflectance now has a redder slope and subdued absorption bands. Note that the mean grain size in the asteoid regolith is smaller than in lunar regolith. Also note that only 1/20 as much SMFe is required to change an ordinary chondrite into an S asteroid as is required to change lunar rock powder into regolith. These results are consistent with the hypothesis that asteroid regoliths are less mature than the Moon's.

Laboratory experiments indicate that on the Moon a time of the order of 100,000 years is required to darken undisturbed lunar rock powder by solar wind sputtering [section 4.3.3]. The sputter - darkening time T_D anywhere else in the solar system is inversely proportional to the solar wind flux Φ averaged over an orbit: $T_D = T_{DM}(\Phi/\Phi_M)$, where T_{DM} is the lunar darkening time, and Φ_M is the average solar wind flux at the moon. Now,

$$\Phi = \frac{1}{P} \int_0^P \frac{\Phi_M}{R^2} dt = \frac{\Phi_M}{P} \int_0^{2\pi} \frac{d\theta}{R^2 \frac{d\theta}{dt}},$$

where R is the distance of the asteriod from the sun in astronomical units (AU), θ is its orbital polar angle, and P is its period of revolution. From Kepler's second law, the denominator of the integrand is a constant of the motion, $R^2 d\theta/dt = 2\pi a^2 \sqrt{(1-e)}/P$, where a is the semimajor axis in AU and e is the eccentricity (see any textbook on celestial mechanics). Thus the integration is trivial, and gives

$$T_D = T_{DM} a^2 \sqrt{(1-e)}. \tag{27}$$

For an asteroid at 3 AU the flux of H ions is smaller by a factor of 10, but only 1/20 as much SMFe is required to change the spectra of a meteorite into an asteroid, so that the time required to alter undisturbed asteroid soil is about 50,000 years. However, just as on the Moon, impacts continuously bury exposed regolith and bring fresh material to the surface, so that the actual time to alter the optical properties is much longer than 50,000 years.

Unless an asteroid has a strong magnetic field, the solar wind bombards its surface, and its spectra must be affected by sputter - deposition of SMFe - rich coatings. Hence, the relevent question is no longer whether or not space weathering occurs on asteroids, but rather, why the spectra of some asteroids appear pristine, while others are heavily altered. Most asteroids probably suffer occasional collisions that are large enough to clear weathered material from their surfaces. This could account for bodies, such as Vesta, which appear to have unweathered surfaces. Another possibility is that the regoliths of apparently - unweathered bodies are composed of large particles > 1 mm in size. Coarse-grained regoliths are much less affected than fine-grained ones [*Hapke*, 1966] because space weathering is mostly a particle surface phenomenon. Asteroids in the outer belt appear to contain large amounts of carbonaceous material. Since these compounds are already dark, space weathering would have less effect on their regoliths. However, it should be noted that a carbonaceous chondrite (Murray) was observed to darken under H ion bombardment [*Hapke*, 1966] (also Table 1), so that some alteration is still expected in the outer belt.

An objection to the mechanism for space weathering of asteroidal regoliths proposed here is that no nonlunar meteorites are known to possess the FMR that characterizes the lunar regolith. This raises the question as to whether any meteorite samples now in our possession are actual samples of asteroid regoliths. Both *McKay et al.* [1989] and *Chapman* [1996] strongly asserted that there are none. Moreover, the FMR is expected to be much weaker in asteroid than in lunar regoliths for two reasons. (1) Only 1/20 as much SMFe is required. (2) Immediately following deposition the SMFe is in the superparamagnetic size range and is too small to cause a large FMR. Postdepositional heating is required (section 5.7), which may be less intense on asteroids because of lower impact velocities.

Although the overall spectrum of the altered ordinary chondrite is similar to the S asteroid, the match is not perfect. In particular, the band centers are at slightly different wavelengths. However, complete agreement is not expected because 26 Proserpina is probably not the parent body of Nanjemoy. In addition, there is a distinct difference between the two spectra that no amount of parameter fiddling will

remove: The absorption bands of 26 Proserpina are considerably broader than Nanjemoy. The only way of doing this, barring some unknown component, is if the asteroid regolith contains glass, since the bands are broader in a glass than in the parent rock (section 3). A significant glass component would also answer the question posed by *Bell et al.* [1989] as to where the parent bodies of the olivine-rich chondrites are: A glass made by vitrifying a pyroxene - poor, olivine - rich material exhibits a 2 μm band and thus could mimic a high - proxene regolith. Because we do not seem to have a good sample of an asteroid regolith in the present meteorite collection, glass-rich regoliths cannot be ruled out. Abundant glass would imply that there is a population of small impactors, probably cometary in orign, hitting asteroid surfaces with a much higher velocity than is commonly believed. *Dohnanyi* [1976] has argued that a signigicant proportion of interplanetary dust in the asteroid belt is cometary.

Another problem is that the short - wavelength shape of the model is insufficiently curved for a perfect match to the asteroid because the SMFe absorption coefficient is not high enough there. A possible resolution to this difficulty may be that the sputter coatings in the asteroid regoliths contain reduced Si and Al. *Dikov et al.* [1978] found reduced Si and Al on the surfaces of lunar soil grains, and *Hapke* [1977] showed that even Fe-free coatings absorb at short wavelengths, which may be caused by reduced Si and Al (section 5.3).

8.5. And Beyond

Although this paper is concerned with space weathering in the inner solar system, the same general process of differentiation by selective loss of heavier atoms during vapor deposition should also occur in the regoliths of bodies in the outer solar system [*Hapke*, 1986]. In particular, deposits of SO_2 frost on Io should experience preferential loss of O by sputter-deposition by Jovian magnetospheric ions, leaving the surface enriched in lower oxides of S, such as polysulfur oxide. The spectra of elemental S and polysulfur oxide are indistinguishable [*Hapke*, 1989].

9. Concluding Remarks

The vapor deposition model of space weathering was proposed in essentially its present form in 1975 by the author and his colleagues, W. Cassidy and E. Wells. However, at that time it was not widely accepted. There were several reasons for this. First, the impact vitrification model of space weathering was simple and seemed eminently reasonable; glass-rich lunar agglutinates are dark; and the effects of Fe^{3+} contamination on the spectrum of glass were not understood. Second, there seemed to be no petrological evidence for vapor deposits in the Apollo soil samples; the coatings discovered in the early TEM images were too thin to be seen through optical microscopes and were dismissed as unimportant by most petrologists. Consequently, the vapor deposition model was ignored, even though the vitrification model became untenable following the publication of the paper by *Wells and Hapke*

[1977], which showed that vacuum-melted glass was not dark. It was not until the recent discovery by Keller and his associates that the coatings are actually SMFe - bearing vapor condensates and the recognition by a number of individuals that the space weathering effects are concentrated in the smaller particles, which implies a surface rather than a volume process, that the vapor deposition model began to be accepted [*Pieters et al.*, 2000].

Twenty-five years ago the interaction of light with a planetary regolith was poorly understood. The development of a theory for light scattering by particulate media has allowed the optical effects of space weathering to be modeled quantitatively. With further modeling it may be possible to remove the effects of space weathering analytically from the spectrum of a regolith to produce a spectrum of the parent rock powder. Lucey and his colleagues [*Blewett et al.*, 1997b; *Lucey et al.*, 1998] have developed a model that estimates the reduction in albedo by space weathering and the FeO and TiO_2 content of lunar regolith. Their model is a good start, but needs to be generalized and better quantified. This would aid in the study of the composition of the lunar crust and in the quest to match meteorites with specific parent asteroids. In order to achieve these goals, better quantitative data are needed, such as the complex refractive index of Fe uncontaminated by oxidation, and the size distribution of Fe particles in the lunar regolith.

References

Adams, J., Interpretation of visible and near-infrared diffuse reflectance spectra of pyroxenes and other rock-forming minerals, in *Infrared and Raman Spectroscopy of Lunar and Terrestrial Minerals*, edited by C. Karr, pp. 91-116, Academic, San Diego, Calif., 1975.

Adams, J., and R. Jones, Spectral reflectivity of lunar samples, *Science*, 167, 737-739, 1970.

Adams, J., and T. McCord, Optical properties of mineral separates, glass, and anorthositic fragments from Apollo mare samples, *Geochim. Cosmochim. Acta, Suppl.*, 2, 2183-2195, 1971.

Adams, J., and T. McCord, Mercury: Evidence for an anothositic crust from reflectance spectra, paper presented at Meeting Am. Astron. Soc. Div. Planet Sci., Honolulu, Hawaii, 1977.

Agrell, S., J. Scoon, I. Muir, J. Long, J. McConnell, and A. Peckett, Observations on the chemistry, mineralogy and petrology of some Apollo 11 lunar samples, *Geochi. Cosmochim. Acta, Suppl.*, 1, 93-128, 1970.

Allen, C., R. Morris, and D. McKay, An experimental analog to maturing lunar soil, *Lunar Planet. Sci.*, *XXVII*, 13-14, 1996a.

Allen, C., R Morris, and D. McKay, Experimental approaches to space weathering, *Lunar Planet. Sci.*, *XXVII*, 15-16, 1996b.

Baron, R., E. Bilson, T. Gold, R. Colton, B. Hapke, and M. Steggert, The surface composition of lunar soil grains: A comparison of results of Auger and X-ray photoelectron [ESCA] spectroscopy, *Earth Planet. Sci. Lett.*, 37, 263-272, 1977.

Baron, R., E. Bilson, T. Gold, R. Colton, B. Hapke, and M. Steggert, Response to comments on "The surface composition of lunar soil grains" by R. M. Housley, Earth, Planet. Sci. Lett., 41, 2471-2472, 1978.

Bell, J., D. Davis, W. Hartmann, and M. Gaffey, Asteroids: The Big Picture, in Asteroids II, edited by R. Binzel, T. Gehrels, and M. Matthews, pp. 921-945, Univ. of Ariz. Press, Tucson, 1989.

Blewett, D., P. Lucey, B. Hawke, G. Ling, and M. Robinson, A comparison of Mercurian reflectance and spectral quantities with those of the Moon, Icarus, 129, 217-231, 1997a.

Blewett, D., P. Lucey, and B. Hawke, Clementine images of the lunar sample return stations: Refinement of FeO and TiO_2 mapping techniques, J. Geophys. Res., 102, 16,319-16,325, 1997b.

Bohren, C., and D. Huffman, Absorption and Scattering of Light by Small Particles, JohnWiley, New York, 1983.

Borg, J., M. Maurette, L. Durrieu, and C. Jouret, Ultramicroscopic features in micron-sized lunar dust grains and cosmophysics, Geochim. Cosmochim. Acta, Suppl., 2, 2027-2040, 1971.

Brandt, J., Introduction to the Solar Wind, W. Freeman, New York, 1970.

Britt, D., and C. Pieters, Darkening in black and gas-rich ordinary chondrites: The spectral effects of opaque morphology and distribution, Geochim. Cosmochim. Acta, 58, 3905-3919, 1994.

Burns, R., Mineralogical Applications of Crystal Field Theory, Cambridge Univ. Press, New York, 1970.

Cadenhead, D., M. Brown, D. Rice, and J Stetter, Some surface area and porosity characterizations of lunar soils, Geochim. Cosmochim. Act, Suppl., 8, 1291-1303, 1977.

Carey, W., and J. McDonnell, Lunar surface sputter erosion: a Monte Carlo approach to microcrater erosion and sputter redisposition, Geochim. Cosnochim. Acta, Suppl., 7, 913-926, 1976.

Carrier, W., G. Olhoeft, and W. Mendell, Physical properties of the lunar surface, in Lunar Sourcebook, edited by G. Heiken, D. Vaniman, and B. French, pp. 475-594, Cambridge Univ. Press, New York, 1991.

Cassidy, W., and B. Hapke, Effects of darkening processes on surfaces of airless bodies, Icarus, 25, 371-383, 1975.

Chapman, C., S-type asteroids, ordinary chondrites and space weathering: The evidence from Galileo's fly-bys of Gaspra and Ida, Meteorit., Planet. Sci., 31, 699-725, 1996.

Cintala, M., Impact induced thermal effects in lunar and Mercurian craters, J. Geophys. Res., 97, 947-974, 1992.

Cisowski, S., The effect of shock on the magnetic properties of natural minerals, Ph.D. dissertation, Univ. of Pittsburgh, Pittsburgh, Pa., 1976.

Cisowski, S., M. Fuller, M. Rose, and P. Wasilewski, Magnetic effects of experimental shocking of lunar soil, Geochim. Cosmochim. Acta, Suppl., 4, 3003-3018, 1973.

Clark, B., F. Fanale, and J. Salisbury, Meteorite-asteroid spectral comparison: The effects of comminution, melting and recrystallization, Icarus, 97, 288-297, 1992.

Cloutis, E., and M. Gaffey, Lunar regolith analogues: Spectral reflectance properties of compositional variations, Icarus, 102, 203-224, 1993.

Cohen, A., Trace ferric iron in lunar and meteoritic titanaugites, Moon, 4, 141-154, 1972.

Conel, J., and D. Nash, Spectral reflectance and albedo of Apollo 11 lunar samples: Effects of irradiation and vitrification and comparison with telescopic observations, Geochim. Cosmochim. Acta, Suppl., 1, 2013-2024, 1970.

DeMaria, G., G. Balducci, M. Guido, and V. Piacente, Mass spectrometric investigation of the vaporization process of Apollo 12 lunar samples, Geochim. Cosmochim. Acta, Suppl., 2, 1367-1380, 1971.

Dikov, Y., O. Bogatikov, V. Barsukov, K. Florensky, A. Ivanov, V. Nemoshkalenko, V. Alyoshin, and M. Chudinov, Some features of the main element conditions in surface layers of the regolith particles of the Luna automatic stations samples: X-ray

photoelectronic spectroscopy studies, Geochim. Cosmochim. Acta, Suppl., 1, 2111-2124, 1978.

Dohnanyi, J., Sources of interplanetary dust: asteroids, in Interplanetary Dust and the Zodiacal Light, edited by H. Elsasser and H. Fechtig, pp. 187-205, Springer-Verlag, New York, 1976.

Dukes, C., R. Baragiola, and L. McFadden, Surface modification of olivine by H^+ and He^+ bombardment, J. Geophys. Res., 104, 1865-1872, 1999.

Dybwad, J., Radiation effects on silicates [5-kev H^+, KD^+, He^+, N_2^+], J. Geophys. Res., 76, 4023-4029, 1971.

Epstein, S., and H. Taylor, D/H and $^{18}O/^{16}O$ ratios of H_2O in the "rusty" breccia 66095 and the origin of "lunar water", Geochim. Cosmochim. Acta, Suppl., 5, 1839-1854, 1974.

Fischer, E., and C. Pieters, Modeling the space weathering - induced optical alteration of lunar soils: First results, Lunar Planet. Sci. Conf., XXV, 371-372, 1994.

Gault, D., F. Horz, and J. Hartung, Effects of microcratering on the lunar surface, Geochim. Cosmochim. Acta, Suppl., 3, 2713-2734, 1972.

Gold, T., The lunar surface, Mon. Not R. Astron. Soc., 115, 585-604, 1955.

Gold, T., M. Campbell, and B. O'Leary, Optical and high-frequency electrical properties of the lunar sample, Geochim. Cosmochim. Acta, Suppl., 1, 2149-2154, 1970.

Gold, T., E. Bilson, and R. Baron, Observation of iron-rich coating on lunar grains and a relation to low albedo, Geochim. Cosmochim. Acta, Suppl., 5, 2413-2422, 1974.

Gold, T., E. Bilson, and R. Baron, Auger analysis of the lunar soil: Study of processes which change the surface chemistry and albedo, Geochim. Cosmochim. Acta, Suppl., 6, 3285-3303, 1975.

Gold, T., E. Bilson, and R. Baron, The surface chemical composition of lunar samples and its significance for optical properties, Geochim. Cosmochim. Acta, Suppl., 7, 901-911, 1976.

Hapke, B., Effects of a simulated solar wind on the photometric properties of rocks and powders, Ann. N. Y. Acad. Sci., 123, 711-721, 1965.

Hapke, B., Optical properties of the Moon's surface, in The Nature of the Lunar Surface, edited by W. Hess, D. Menzel, and J. O'Keefe, pp. 141-154, Johns Hopkins Univ Press, Baltimore, Md., 1966.

Hapke, B., The composition of the lunar surface inferred from optical properties, Science, 159, 76-79, 1968.

Hapke, B., Darkening of silicate rocks by solar wind sputtering, Moon, 7, 342-355, 1973.

Hapke, B., Interpretations of optical observations of Mercury and the Moon, Phys. Earth, Planet. Inter., 15, 264-274, 1977.

Hapke, B., On the sputter alteration of regoliths of outer solar system bodies, Icarus, 66, 270-279, 1986.

Hapke, B., The surface of Io: a new model, Icarus, 79, 56-74, 1989.

Hapke, B., Theory of Reflectance and Emittance Spectroscopy, Cambridge Univ. Press, New York, 1993a.

Hapke, B., Why is the Moon dark?, Lunar Planet. Sci. XXIV, 605-606, 1993b.

Hapke, B., How to turn OC's into S's: Space weathering in the asteroid belt, Lunar Planet. Sci. [CD-ROM], XXXI, abstract 1087, 2000.

Hapke, B., and W. Cassidy, Is the Moon really as smooth as a billiard ball? Remarks concerning recent models of sputter-fractionation on the lunar surface, Geophys. Res. Lett., 5, 297-300, 1978.

Hapke, B., and H. Van Horn, Photometric studies of complex surfaces, with applications to the Moon, J. Geophys. Res., 68, 4545-4570, 1963.

Hapke, B., and E. Wells, Bidirectional reflectance spectroscopy, 2., Experiments and observations, J. Geophys. Res., 86, 3055-3060, 1981.

Hapke, B., A. Cohen, W. Cassidy, and E. Wells, Solar radiation effects on the optical properties of Apollo 11 lunar samples, Geochim. Cosmochim. Acta, Suppl., 1, 2199-2212, 1970.

Hapke, B., W. Cassidy, and E. Wells, Effects of vapor-phase deposition

processes on the optical, chemical and magnetic properties of the lunar regolith, *Moon, 13,* 339-354, 1975a.

Hapke, B., G. Danielson, K. Klaasen, and L. Wilson, Photometric observations of Mercury from Mariner 10, *J. Geophys. Res., 80,* 2431-2443, 1975b.

Hapke, B., W. Cassidy, and E. Wells, Vapor deposits in the lunar regolith, *Science, 264,* 1779-1780, 1994.

Heiken, G., D. Vaniman, and B. French, *Lunar Sourcebook,* Cambridge Univ. Press, New York, 1991.

Horz, F., and R. Schaal, Asteroidal agglutinate formation and implications for asteroidal surfaces, *Icarus, 46,* 337-353, 1981.

Housley, R., and R. Grant, ESCA studies of lunar surface chemistry, *Geochim. Cosmochim. Acta, Suppl., 6,* 3269-3275, 1975.

Housley, R., and R. Grant, ESCA studies of the surface chemistry of lunar fines, *Geochim. Cosmochim. Acta, Suppl., 7,* 881-889, 1976.

Housley, R., and R. Grant, An XPS [ESCA] study of lunar surface alteration profiles, *Geochim. Cosmochim. Acta, 8,* 3885-3899, 1977.

Housley, R., R. Grant, and N. Paton, Origin and characteristics of excess Fe metal in lunar glass welded aggregates, *Geochim.Cosmochim. Acta, Suppl., 4,* 2737-2749, 1973.

Housley, R., E. Cirlin, I. Goldberg, and H. Crowe, Ferromagnetic resonance studies of lunar core stratigraphy, *Geochim. Cosmochim. Acta, Suppl., 7,* 13-26, 1976.

Johnson, P., and R. Christy, Optical constants of transition metals: Ti, V, Cr, Mn, Fe, Co, Ni and Pd, *Phys. Rev., B9,* 5056-5070, 1974.

Johnson, R., and R. Baragiola, Lunar surface: Sputtering and secondary ion mass spectrometry, *Geophys. Res. Lett., 18,* 2169-2172, 1991.

Keller, L., and D. McKay, Discovery of vapor deposits in the lunar regolith, *Science, 261,* 1305-1307, 1993.

Keller, L., and D. McKay, The nature and origin of rims on lunar soil grains, *Geochim. Cosmochim. Acta, 61,* 2331-2340, 1997.

Keller, L., S. Wentworth, D. McKay, L. Taylor, C. Pieters, and R. Morris, Space weathering in the fine size fraction of lunar soils: Mare/highland differences, *Lunar Planet. Sci.* [CD-ROM], *XXXI,* abstract 1655, 2000.

KenKnight, C., D. Rosenberg, and G. Wehner, Parameters of the optical properties of the lunar surface powder in relation to solar wind bombardment, *J. Geophys. Res., 72,* 3105-3130, 1967.

Kerridge, J., Production of superparamagnetic Fe⁰ on the lunar surface, *Lunar Planet. Sci. XXV,* 695-696, Houston, 1996.

Lucey, P., D. Blewett, and B. Hawke, Mapping the FeO and TiO_2 content of the lunar surface with multispectral imagery, *J. Geophys. Res. 103,* 3679-3699, 1998.

Mao, H., D. Virgo, and P. Bell, Analytical and experimental study of iron and titanium in orange glass from Apollo 17 soil sample 74220, *Geochim. Cosmochim Acta, Suppl., 4,* 397-412, 1973.

Maurette, M., and P. Price, Electron microscopy of irradiation effects in space, *Science, 187,* 121-129, 1975.

McCord, T., and J.Adams, Mercury: Surface composition from the reflection spectrum, *Science, 178,* 745-774, 1972.

McDonnell, J., Accreting particle studies on Apollo 12054,58: In-situ lunar surface microparticle flux rate and solar wind sputter rate defined, *Geochim. Cosmochim. Acta, Suppl., 8, 3835-3957, 1977.*

McKay, D., R. Fruland, and G. Heiken, Grain size and the evolution of lunar soils, *Geochim. Cosmochim. Acta, Suppl., 5,* 887-906, 1974.

McKay, D., T. Swindle, and R. Greenberg, Asteroidal regoliths: What we do not know, in *Asteroids II,* edited by R. Binzel, T. Gehrels, and M. Matthews, pp. 617-642, Univ. of Ariz. Press, Tucson, 1989.

Morgan, T., H. Zook, and A. Potter, Production of sodium vapor from exposed regolith in the inner solar system, *Proc. Lunar Planet. Sci. Conf., 19th,* 297-304, 1989.

Moroz, L., A. Fisenko, L. Semjonova, C. Pieters, and N. Korotaeva, Optical effects of regolith processes on S-asteroids as simulated by laser shots on ordinary chondrite and other mafic materials, *Icarus, 122,* 366-382, 1996.

Morris., R., Surface exposure indices of lunar soils: A comparative FMR study, *Geochim. Cosmochim. Acta, Suppl., 7,* 315-335, 1976.

Morris, R., Origin and evolution of the grain-size dependence of the concentration of fine-grained metal in lunar soils: the maturation of lunar soils to a steady-state stage, *Geochim. Cosmochim. Acta, Suppl., 8,* 3719-3747, 1977.

Morris, R., Origin and size distribution of metallic iron particles in the lunar regolith, *Geochim. Cosmochim. Acta, Suppl., 14,* 1697-1712, 1980.

Morris, R., R. Gibbons, and F. Horz, Ferromagnetic resonance and magnetic studies up to 900 C of lunar soils and potential magnetic analogs, *Geophys. Res. Lett., 2,* 461-464, 1975.

Nash, D., Proton irradiation darkening of rock powders: Contamination and temperature effects, and applications to solar wind darkening of the Moon, *J. Geophys. Res., 72,* 3089-3104, 1967.

Noble, S., C. Pieters, L. Taylor, R. Morris, C. Allen, D. McKay, and L. Keller, The optical properties of the finest fraction of lunar soils: Implications for space weathering environments, *Meteorit. Planet. Sci., 36,* 31-42, 2001.

Papike, J., S. Simon, C. White, and J. Laul, The relationship of the lunar regolith < 10 μm fraction and agglutinates: A model for agglutinate formation and some indirect supportive evidence, *Geochim. Cosmochim. Acta, Suppl., 16,* 409-420, 1982.

Paruso, D., W. Cassidy, and B. Hapke, An experimental investigation of fractionation by sputter deposition, *Geochim. Cosmochim. Acta, Suppl., 10,* 1711-1724, 1978.

Pearce, G., R. Williams, and D. McKay, The magnetic properties and morphology of metallic iron produced by subsolidus reduction of synthetic Apollo 11 composition glasses, *Earth Planet Sci. Lett., 17,* 95-104, 1972.

Pieters, C., E. Fischer, O. Rode, and A. Basu, Optical effects of space weathering: The role of the finest fraction, *J. Geophys. Res., 98,* 20,817-20,824, 1993.

Pieters, C., L. Taylor, S. Noble, L. Keller, B. Hapke, R. Morris, C. Allen, D. McKay, and S. Wentworth, Space weathering on airless bodies: Resolving a mystery with lunar samples, *Meteorit. Planet. Sci., 35,* 1101-1107, 2000.

Pillinger, C., L. Gardiner, and A. Jull, Preferential sputtering as a method of producing metallic iron, inducing major element fractionation and trace element enrichment, *Earth Planet. Sci. Lett., 33,* 289-299, 1976.

Rava, B., and B. Hapke, An analysis of the Mariner 10 color ratio map of Mercury, *Icarus, 71,* 397-429, 1987.

Rosenberg, D., and G. Wehner, Darkening of powdered basalt by simulated solar wind bombardment, *J. Geophys. Res., 69,* 3307-3308, 1964.

Shkuratov, Y., and L. Starukhina, A model of spectral albedo of particulate surfaces: implications for optical properties of the Moon, *Icarus, 137,* 235-246, 1999.

Starukhina, L., Y. Shkuratov, O. Rode, and C. Pieters, Reflectance spectra of particle size separates of lunar soils: Is the difference controlled by reduced iron?, *Lunar Planet. Sci., XXV,* 1333-1334, 1994.

Starukhina, L., Y. Shkuratov, and S. Skorik, Spread of condensation products in a regolith-like medium: estimates and laboratory modeling, *Solar Syst. Res., 33,* 212-215, 1999.

Stull, D., and H. Prophet, *JANAF Thermochemical Tables, Publ.* NSRDS-NBS 37, U.S. Gov. Printing Off.,Washington, D. C., 1971.

Tarng, M., and G Wehner, Alloy sputtering studies with in situ auger electron spectroscopy, *J. Appl. Phys., 42,* 2449-2452, 1971.

Taylor, L., C. Pieters, R. Morris, L. Keller, D. McKay, A. Patchen, and S. Wentworth, Integration of the chemical and mineralogical characteristics of lunar soils with reflectance spectroscopy, in *Lunar Planet. Sci.* [CD-ROM], *XXX,* abstract 1859, 1999a.

Taylor, L., A. Patchen, R. Morris, D. Taylor, C. Pieters, L. Keller, D. McKay, and S. Wentworth, Chemical and mineralogical characterization of the 44-20, 20-10 and < 10 micron fractions of lunar mare soils, *Lunar Planet. Sci.* [CD-ROM], *XXX,* abstract 1885, 1999b.

Vilas, F., Surface composition of Mercury from reflectance spectrophotometry, in *Mercury,* edited by F. Vilas, C. Chapman, and M. Matthews, pp. 59-76, Univ. of Ariz. Press, Tucson, 1988.

Vinogradov, A., V. Nefedov, V. Urusov, and N. Zhavoronkov, ESCA-investigation of lunar regolith from the Seas of Fertility and Tranquility, *Geochim. Cosmochim. Acta, Suppl., 3*, 1421-1427, 1972.

Wagner, J., B. Hapke, and E. Wells, Atlas of reflectance spectra of terrestrial, lunar and meteoritic powders and frosts from 90 to 1800 nm, *Icarus, 69*, 14-28, 1987.

Wehner, G. Influence of the angle of incidence on sputtering yields, *J. Appl. Phys., 30*, 1762-1765, 1959.

Wehner, G. Sputtering effects on the Moon's surface, *Am. Rocket Soc. J., 31*, 438-439, 1961.

Wehner, G., Sputtering effects on the lunar surface, in *The Lunar Surface Layer*, edited by J. Salisbury, and P. Glaser, pp. 313-322, Academic, San Diego, Calif., 1964.

Wehner, G., C. KenKnight, and D. Rosenberg, Sputtering rates under solar wind bombardment, *Planet. Space Sci., 11*, 885-895, 1963.

Wells, E., and B. Hapke, Lunar soil: Iron and titanium bands in the glass fraction, *Science, 195*, 977-979, 1977.

Wentworth, S., L. Keller, D. McKay, and R. Morris, Space weathering on the Moon: Patina on Apollo 17 samples 75075 and 76015, *Meteorit. Planet. Sci., 34*, 593-603, 1999.

Yamada, M., S. Sasaki, H. Nagahara, A. Fujiwara, S. Hasegawa, H.

Yano, T. Hiroi, H. Ohashi, and H. Otake, Simulation of space weathering of planet-forming materials: Nanosecond pulse laser irradiation and proton implantation on olivine and pyroxene samples, *Earth Planets Space, 51*, 1255-1265, 1999.

Yin, L., and T. Tsang, On the ion bombardment reduction mechanism, *Geochim. Cosmochim. Acta, Suppl., 7*, 891-900, 1976.

Yin, L., S. Ghose, and I. Adler, Investigation of a possible solar wind darkening of the lunar surface by photoelectron spectroscopy, *J. Geophys. Res., 77*, 1360-1367, 1972.

Yin, L., T. Tsang, and I. Adler, ESCA studies on solar wind reduction mechanisms, *Geochim. Cosmochim. Acta, Suppl., 6*, 3277-3284, 1975

Zook, H., and J. McCoy, Large scale lunar horizon glow and a high altitude lunar dust exosphere, *Geophys. Res. Lett., 18*, 2117-2120, 1991.

B. W. Hapke, 321 Old Engineering Hall, University of Pittsburgh, Pittsburgh, PA 15260. (hapke@pitt.edu)